The Effect of Stromal Components on the Phenotype of Normal Human Bronchial Epithelial Cells in 3D Culture

A dissertation
submitted by

Steven C. Pageau

In partial fulfillment of the requirements of
Doctor of Philosophy

in

Cell, Molecular and Developmental Biology

TUFTS UNIVERSITY

Sackler School of Graduate Biomedical Sciences

August, 2011

ADVISORS: Ana Soto and Carlos Sonnenschein

ABSTRACT

Classical studies in embryology demonstrated that stroma is necessary for the proper specification and differentiation of epithelial tissues. Recently, it was shown that the stroma is involved in the homeostatic maintenance of adult tissues, and under pathologic conditions, promotes the development and progression of diseases such as cancer. Hence, pulmonary diseases such as asthma, fibrosis and cancer can be understood in the context of altered communications between the epithelial and stromal tissue compartments.

Bronchi are the conducting airways of the lung. Bronchi trap and eliminate inhaled particles through the coordinated actions of mucus secretion and the beating of cilia. However, inhaled toxicants and carcinogens are linked to several broncho-pulmonary pathologies, including asthma and lung cancer, which is the single deadliest cancer in the United States; since most lung cancers are attributed to tobacco smoke, it is also one of the most avoidable of cancers.

This thesis describes the construction of an *in vitro* three-dimensional (3D) model of the human bronchus specifically designed for the study of epithelial-stromal interactions that regulate bronchial homeostasis and pathogenesis. This model mimics the morphology and function of the bronchial mucosa and consists of a type-I collagen matrix, either normal human fetal lung fibroblasts (IMR-90) or primary human adult lung cancer-associated fibroblasts (LuCAFs), and a surface epithelium of normal human bronchial epithelial cells (HBECs). When cultured at an air-liquid interface (ALI), the epithelium generated a well-differentiated pseudostratified bronchial epithelium that

contained basal, ciliated, and non-ciliated (secretory) epithelial cells. IMR-90 and LuCAFs differentially altered the phenotype of HBECs in distinct ways. While IMR-90 permitted HBECs to form a typical respiratory surface epithelium, LuCAFs promoted the invasion of HBECs into collagen gel forming both epithelial nodules and cysts. This suggests that LuCAFs may alter the HBEC phenotype by modifying biomechanical signals conveyed through the extracellular matrix (ECM). Furthermore, LuCAFs secreted soluble factors that induced HBECs to express genes associated with immune responses, apoptosis, mitosis, cell survival, differentiation and cancer. In conclusion, we have created a 3D model of the human bronchial mucosa that allows investigators to study epithelial-mesenchymal interactions as determinants of tissue architecture as well as the effects of inhaled toxicants.

ACKNOWLEDGEMENTS

Many factors influenced my decision to pursue a doctoral degree in Cell, Molecular and Developmental Biology at the Tufts University Sackler School of Graduate Biomedical Sciences, but my principal motivator was intellectual curiosity. Since childhood, I've have had a zeal for the fascinating complexity of biological systems. Advanced scientific degrees are often fraught with countless experimental failures and fewer successes, and my experience was no exception to this rule. I have many people to thank for talking me through my moments of self-doubt, and for helping me to reach the end of my graduate studies.

I would like to thank the Tufts University Sackler School of Graduate Biomedical Research Sciences for creating an outstanding academic environment and for supporting scientific training. I would like to thank Dr. John Castellot, Director of the Cell, Molecular and Developmental Biology Program, for his leadership and role in designing a superior academic program. I would like to sincerely thank my thesis advisors, Drs. Ana Soto and Carlos Sonnenschein. Ana and Carlos were true mentors in every sense of the word. They provided me with knowledge, advice and guidance. They nurtured my individual interests and supported my thesis research project from start to finish. I would like to thank my Thesis Advisory Committee for their commitment of time and wisdom, and for helping me to develop an interesting and informative thesis project. I would like to thank and acknowledge Dr. Scott Randell and Leslie Fulcher at the University of North Carolina, Chapel Hill, for providing me with air-liquid interface culture training and the many generous gifts of materials. I would like to thank all of my collaborators, but

especially Drs. Joyce Wong and Olga Sazonova of the Department of Biomedical Engineering at Boston University for their assistance with atomic force microscopy studies. I would like to thank my classmates and colleagues for the many conversations that helped to broaden and enrich my thoughts, and members of my laboratory for their help and encouragement.

Of course, I would like to thank my family for their support. My parents, for the gift of life and for their many teachings which shaped the person I am today. I would like to thank my siblings for their advice which I typically ignored. I would like to thank my in-laws for always taking the time to understand my research, and for enthusiastically supporting my academic pursuits. Not to be forgotten, I would like to thank my loving wife, Isla, for her unwavering support and for the many sacrifices she made so that I could achieve my goal. Her greatest gift and personal sacrifice was granting me the time to complete my degree, and for that I am eternally grateful. Lastly, I would like to honor my many family members and friends who have courageously battled serious illnesses. I hope that one day my efforts may help in some way to diminish the suffering caused by disease.

TABLE OF CONTENTS

LIST OF TABLES

LIST OF FIGURES

CHAPTER 1

INTRODUCTION

A goal of every biologist -- myself included -- is to understand why and how biological processes occur, regardless of whether the events are normal or abnormal. To study human development and disease, we select models which are thought to faithfully replicate human biology. Animal models have taught us about embryonic development and the impact that toxic and carcinogenic compounds have on tissues and organ systems. Unfortunately, a serious limitation of laboratory animals is that toxicants and carcinogens that are known to cause human disease sometimes fail to have a similar effect in animals. Furthermore, when disease results, we often lack the technical ability to define the events that transpire at the moment a tissue converts from a normal to an abnormal phenotype, a constraint identified in 1914 by the German biologist Theodor Boveri when he stated that cancer cannot be observed "*in statu nascendi*".

To resolve this shortcoming, two-dimensional (2D) cell culture has been offered as a reductionist solution. 2D cell culture relies upon cells which have been isolated from either normal or pathological tissue specimens, and adapted for growth on a plastic surface in an artificial *in vitro* environment. While it was once thought that 2D cell culture would create a windfall of data and lead to a detailed comprehension of the intracellular events that lead to organismal dysfunction, it has become clear that 2D cell culture does not replicate the complexity of living systems. For example, epithelial cells grown on 2D surfaces generally form flat monolayers, fail to secrete basement membrane proteins, and lack both morphological and functional specification. Furthermore, the

phenotype of epithelial cells varies widely depending upon whether they are cultured on rigid or compliant surfaces. Consequently, results gathered using 2D cell culture are often artifactual and may lead to incorrect conclusions.

Cells display different phenotypes when cultured on either a hard or a soft substrate. The field of biomechanics, which is the study of the mechanical properties of living organisms, has long appreciated that cellular function can be influenced by tissue mechanics. A prime example of this is the skeletal-muscular system. As skeletal muscles contract, forces are transmitted through tendons to their areas of insertion on bones, causing osteoblasts to secrete additional bone matrix at the sites of insertion. Mechanotransduction, or the transmission of physical force at the cellular level, influences cellular chemistry and phenotype in the absence of exogenous biochemical messengers [1]. Just as physical forces help to maintain the homeostasis of tissues, they may also promote their pathogenesis. Fibrosis is a condition in which fibroblasts secrete collagens abnormally in a manner that stiffens the tissue, causing parenchymal dysfunction. Therefore, when engineering *in vitro* surrogate models to represent living tissues, one must consider several design principles, including both cellular and acellular composition and whether cells receive the appropriate mechanical cues from their matrix.

In line with these facts, we contend that normal and abnormal development are processes that are not regulated at a cellular or intracellular level of biological organization, but rather at the tissue organizational level [2]. In addition, evidence collected in this lab using tissue recombination in rodents suggests that the stroma, rather than the epithelium, is the target of chemical carcinogens [3, 4]. In order to overcome the technological gap that exists between animal models and 2D cell culture, members of the

lab and I have developed three-dimensional (3D) models of human tissues that contain both a parenchyma and stroma, with which we can observe both normal tissue morphogenesis and pathogenesis.

The thesis that follows details the creation of a 3D model of the human bronchial mucosa which allowed us to understand how cellular and acellular stromal elements combined to support the differentiation of a functional and morphologically satisfactory epithelium. In addition, we utilized this model to explain how changes to the stroma – whether they be changes in the composition and/or concentration of extracellular matrix proteins, or the inclusion of cancer-associated fibroblasts – promoted the epithelium to adopt an abnormal morphology and exhibit behaviors reminiscent of a bronchial epithelial cancer. Several variables were tested and we believe that our results will be valuable to researchers wishing to study bronchial pathologies and to those who aspire to develop 3D surrogate models of human tissues.

CHAPTER 2

BACKGROUND AND LITERATURE REVIEW

2.1 Epithelial-Mesenchymal Interactions Regulate Lung Morphogenesis

Human lung development has been divided into five stages: *(1)* the embryonic stage (3 to 6 weeks of gestation), during which a primitive lung bud arises from the foregut and divides into two distinct primordial lung buds, which then elongate caudally into the primitive mesenchyme; *(2)* the pseudo-glandular stage (6 to 16 weeks of gestation), during which signaling from the lung mesenchyme drives a successive series of bronchiolar budding and branching events, ultimately resulting in the formation of a respiratory tree with terminal bronchioles; *(3)* the canalicular stage (16 to 28 weeks of gestation), during which the lung vasculature develops and terminal bronchioles give rise to respiratory bronchioles complete with terminal sacs; *(4)* the saccular stage (28 to 36 weeks of gestation), during which primitive alveoli lined with type I alveolar epithelial cells develop (AECs); *(5)* and the alveolar stage (36 weeks of gestation to 4 years of age), during which the development of mature alveoli and the respiratory vasculature continues to completion [5].

Mouse lung development is remarkably similar to human lung development. Therefore, the embryonic murine lung has been a choice model with which to study the mechanisms that control branching morphogenesis and the epithelial-mesenchymal signaling interactions that regulate organogenesis. In mouse embryos, two lung buds originate as an epithelial outgrowth from the ventral foregut and undergo a period of branching while the epithelium invades the surrounding splanchnic mesoderm. There are

four discrete chronological stages of murine lung development: *(1)* the pseudo-glandular stage (E9.5 to E16.6), during which the bronchial and respiratory tree develops and primordial cells and structures become specified; *(2)* canalicular stage (E16.6 to E17.4), during which terminal sacs and the lung vasculature develop; *(3)* the terminal sac stage (E17.4 to P5), which is typified by increased vascularization, greater numbers of terminal sacs, and the appearance of differentiated type I and II AECs; and *(4)* the alveolar stage (P5 to P30), during which the terminal sacs develop into mature alveolar ducts and alveoli [5].

Physical and biochemical interactions between the epithelium and mesenchyme regulate the development and differentiation of tissues and organs, and numerous studies have demonstrated the critical importance of the mesenchyme in lung development [6, 7]. Classical experiments performed by Rudnick, in which embryonic chicken lung rudiments were cultured *in ovo* on chorioallantoic membranes, showed that normal branching occurred as long as the rudiments were grafted with their associated mesenchyme [8]. Five decades later, using rodent embryonic tissues, Wessels and Lawson demonstrated that salivary mesenchyme supported the branching morphogenesis of embryonic lung buds, and lung mesenchyme induced the branching of salivary epithelium [9-11]. These studies were followed by the pioneering publication by Sakakura *et al.* which demonstrated that embryonic mammary mesenchyme provided sufficient cues to induce the salivary epithelium to morphologically differentiate into a mammary gland-like structure [12]. More recently, Shannon *et al.* demonstrated that the rat distal embryonic splanchnic mesoderm promoted the proximal rudimentary lung epithelium to develop into a distal alveolar phenotype, while the recombination of

proximal mesenchyme with distal lung epithelium induced a proximal tracheal phenotype [13, 14]. Together, these studies demonstrate that stroma is necessary for the induction of organogenesis and the specification of the epithelium.

2.2 Functional Anatomy and Histology of the Human Bronchus

The bronchi are the proximal conducting airways of the lung that extend from the trachea to the distal portions of the respiratory tree where gas exchange occurs. In addition to serving as a conduit, the bronchi condition inspired air and trap noxious and harmful particles. Four main tissue layers comprise the bronchi: a mucosa, consisting of a pseudostratified, ciliated, columnar epithelium positioned upon a lamina propria; a thin band of connective tissue and smooth muscle termed the muscularis mucosae; a submucosa consisting of connective tissue, cartilage and submucosal glands; and the outermost connective layer, the adventitia [15, 16]. Several epithelial cell types are contained within the mucosa. Goblet and ciliated epithelial cells extend from the basement membrane to the apical surface of the airway lumen. Goblet cells secrete carbohydrate-rich mucins, which combine with secretions from the submucosal glands to form the mucus that traps inhaled foreign particles. The coordinated beating of cilia on the surface of ciliated epithelial cells moves the mucus and any trapped particles upward through the conducting airway and toward the pharynx, where it can be expelled. Basal epithelial cells are positioned immediately above and on top of the basement membrane. Basal cells are the only cells within the bronchial mucosa which are capable of forming hemi-desmosomes [17]. Therefore, a major role for basal cells is to enhance the anchorage of columnar epithelial cells within the tissue through direct desmosomal

connections. In the bronchial mucosa, goblet, ciliated and basal epithelial cells comprise 15%, 47%, and 32% of the total epithelial cell population, respectively [15]. The remaining 6% is represented by minor cell types, such as neuroendocrine cells (NEC), brush cells, and intermediate cells which defy precise characterization.

The basement membrane zone lies directly beneath the mucosa and attaches the bronchial epithelium to the extracellular matrix (ECM) . The basement membrane zone can be divided into three distinct layers based on their molecular composition and ultrastructural appearance [18, 19]. The lamina lucida is abundant in adhesion filaments, such as laminin 5. The lamina densa is comprised of type IV collagen, laminins, proteoglycans, and entactin (nidogen-1). Together, the lamina lucida and the lamina densa form the basal lamina. Below the basal lamina is the lamina reticularis, which is rich in structural ECM proteins including collagens I, III, V, VI and VII, and nonstructural proteins such as fibronectin, tenascin and proteoglycans. It is within the lamina reticularis that collagen accumulation occurs in fibrotic airway diseases, such as asthma [20] .

Closely opposed to the lower margin of the lamina reticularis is a dense layer of fibroblasts and myofibroblasts referred to as the attenuated fibroblast sheath [21]. Fibroblasts and cell processes can be seen throughout the lamina reticularis, and in some cases, make contact with the lamina densa. Though the function of fibroblasts within the attenuated sheath is unknown, much can be inferred from their anatomical position. It is thought that they may assist in the homeostatic maintenance of the bronchial ECM through the secretion of structural proteins [22]. They may serve as a communication link between cells of the mucosa and submucosa [21]. Another plausible alternative is that

they may aid in the response to injury, allergens, pathogens, and toxic stress through the secretion of cytokines [23, 24].

2.3 Epidemiology and Pathogenesis of Human Lung Cancer

Approximately 175,000 persons are diagnosed with lung cancer annually in the US, and most of them will die from their disease, making lung cancer the number one cancer killer in the US today [25]. The majority of lung cancers are classified as non-small cell lung cancers (NSCLCs), which typically arise in the conducting airways of the lung (bronchi and bronchioles) [26]. Pathologically, NSLCs are a heterogeneous group of cancers that predominantly consist of squamous cell carcinoma and adenocarcinoma subtypes [27, 28]. From a clinical perspective, based on radiological and computed tomography (CT) screening, it is becoming increasingly apparent that lung cancer is not a monolithic entity. Even if left untreated, early-stage lung neoplasms do not always progress into advanced cancers that cause clinical disease and death [29-31]. Analysis of epidemiological data suggests instead that there is a bimodal distribution of lung cancers whereby histologically confirmed early-stage lung cancer represents a different clinical entity from the advanced lung cancer usually detected at the end of the carcinogenic process, shortly before the patient's death [32]. This suggests that our understanding of the natural history of NSCLCs is incomplete and should be refined.

2.4 Tobacco Use and its Link to Human Lung Cancer

Archaeologists estimate that tobacco cultivation and consumption in the Americas dates to at least 6000 BC [33]. However, tobacco was not conclusively identified as a

cause of human disease until 1950, when a link between cigarette smoking and lung cancer was established [34]. In 1964, the United States Surgeon General presented a comprehensive and compelling report on cigarette smoking and its association with lung cancer [35]. At that time, nearly 50% of the US adult population smoked tobacco, and almost half-a-century later, this percentage remains steady at 25% despite anti-smoking campaigns and compelling evidence connecting cigarette smoking to human morbidity and mortality. With over one billion persons actively smoking worldwide, the diseases it causes have reached epidemic proportions [36].

Inhaled tobacco smoke contains more than 10^{10} particles/ml [37]. Researchers have tried to identify which of the more than 3500 compounds within the particulate phase of mainstream (inhaled) cigarette smoke cause cancer in humans. Over 20 of these compounds have been shown to cause lung tumors in experimental laboratory animals. Two of the most abundant tobacco carcinogens are the polyaromatic hydrocarbon benzo[a]pyrene (BaP) and the nicotine-derived nitrosomine 4-(methylnitrosamino)-1-(3-pyridyl)-1-butanone (NNK) [38]. When administered systemically in mice, BaP causes squamous cell carcinoma-like pulmonary lesions [39]. In contrast, either systemic or intratracheal administration of NNK results in pulmonary adenomas and adenocarcinomas in several rodent species [40]. While these studies established a positive correlation between cigarette carcinogen exposure and lung cancer in rodents, whole smoke inhalation studies have been less successful. To date, no smoke inhalation study has been able to demonstrate that cigarette smoke exposure causes tumors in rodents [41]. Possible reasons for these failures are that animals display avoidance to smoke and that rodents are obligate nose breathers. Combined with varying susceptibility and resistance

to carcinogens seen among rodents, it has become clear that a suitable surrogate model for the human lung must be identified if we are to truly comprehend the toxicity of complex mixtures, such as cigarette smoke.

2.5 Biomechanics and Stroma Regulate Pulmonary Function and Pathology

The lung is an elastic organ that is constantly undergoing periodic distortion and relaxation due to respiration. Physical forces generated during respiration are transmitted through the extracellular matrix to parenchymal and stromal cells, thereby altering cellular biochemistry and phenotype [42]. In the lung, fibrillar collagens are the principle load-bearing connective tissue elements of the lung, and therefore, are largely responsible for mechanotransduction [1]. Peripherally, mechanical stress causes alveolar epithelial cells to secrete pulmonary surfactants and interstitial fibroblasts to secrete extracellular matrix proteins [6, 43-45]. Proximally, physical strain causes tracheal epithelial cells to alter their ciliary beat frequency [46]. In addition to regulating normal lung physiology, evidence suggests that physical forces may be responsible for the development of several lung pathologies.

In the lung, stromal dysplasia is a distinctive feature of various adult respiratory diseases such as asthma, emphysema, chronic obstructive pulmonary disease (COPD), pulmonary fibrosis and lung cancers. Asthma is a broncho-pulmonary disease that can be characterized by upper airway inflammation, airway constriction, and structural changes in the airway wall due to airway remodeling. Induced bronchoconstriction on the airway is sufficient to induce a thickening of the bronchial stroma in asthmatic patients, which has been correlated with decreased bronchial function and poor clinical outcomes [47]. A

progressive loss of alveoli is a hallmark of emphysema, COPD and pulmonary fibrosis, and may be preceded and superseded by a thickening of the alveolar interstitial walls due to the presence of myofibroblasts and the fibrillar collagens they secrete [20, 48-50]. Several recent studies have correlated the activities of pulmonary fibroblasts with the emergence and progression of lung cancer [51-53].

The stroma is important for the homeostatic maintenance of other tissues and organs. Using a rodent model of mammary gland carcinogenesis and tissue recombination techniques, Maffini *et al*. showed that carcinogen-exposed rat mammary stroma induced normal unexposed mammary epithelial cells to develop into neoplasias [4]. Conversely, unexposed mammary stroma induced mammary tumor cells to differentiate into normal mammary ducts [3]. Sufficient evidence buttresses the prominent role of the stroma in carcinogenesis at large [2] and in other degenerative diseases [54-56].

2.5.1 Cancer Associated Fibroblasts

If a carcinogen-exposed stroma is sufficient to cause the development of mammary neoplasias, then one can infer that the carcinogen may have altered the cellularity of the stroma and/or the ability of stromal cells to communicate in either a biochemical, biophysical or spatial context with themselves or their adjacent epithelium. Data collected on fibroblasts isolated from the peri-tumor margin suggest that stromal cells may promote tumor initiation and progression [57-59]. Other studies have described cancer associated fibroblasts (CAFs) as “activated” myofibroblasts with abnormal morphologies and migratory behaviors [60]. Under normal homeostatic circumstances,

fibroblasts secrete ECM proteins, such as type-I collagen, in a manner that maintains the integrity and functionality of tissues. However, fibroblasts activated under pathologic conditions alter the composition and mechanics of the ECM, and thereby may promote pathogenesis.

2.6 Human Bronchial Cell Lines for Air-Liquid Interface Studies

The development of air-liquid interface (ALI) culture techniques have allowed researchers to design *in vitro* models that mimic tissues that are normally exposed to air, such as skin, airway, oral cavity and cornea [61-64]. Nonetheless, numerous obstacles, some inherent to biological research models, prevent using standardized cells (cell strains and cell lines) to draw robust conclusions regarding their roles in development and disease. Cell lines have some advantages over primary cells. On the one hand, established cell lines provide researchers with a reasonable supply of cell types derived from a variety of normal and diseased tissues. They can be obtained either free or at a modest cost from public, private and commercial sources. They have been adapted to grow in commonly available culture media using standard techniques. They exhibit less genotypic and phenotypic variability in culture than primary cells, which may have been isolated from several unrelated donors. Cell lines from commercial repositories are typically screened for viral, prokaryotic, and fungal contaminants, as well as other contaminating cell lines. And perhaps most importantly, cell lines may be propagated nearly indefinitely, while primary cells often cease to proliferate and exhibit phenotypic changes in culture after a few passages.

However, on the other hand, established cell lines have limitations. They are often aneuploid and may possess chromosomal abnormalities that are rarely if ever observed in their original hosts. Cell lines may display accelerated growth kinetics and a lack of contact inhibition in culture. They may have been adapted for growth on rigid substrates with media that may contain undefined supplements, such as animal serum. They may have been derived from tumor biopsies, and may retain the capacity to form tumors when injected into immunocompromised laboratory animals. Cell lines may be contaminated with viruses, prokaryotes, fungi, or even worse, by other cell types (see Appendix II). Lastly, and most importantly, they rarely retain the ability to form physiologically relevant, functional, specialized tissues when cultured *in vitro*.

Several tracheo-bronchial epithelial cell lines have been used by the pulmonary research community for studies of bronchial barrier function, drug transport and metabolism, and inhalation toxicology [65]. Those most frequently reported are Calu-3, 16HBE14o-, and BEAS-2. Calu-3 was derived from a pulmonary adenocarcinoma and exhibits several morphologic and phenotypic properties of a bronchial epithelial cell, including tight junction formation, expression of the cystic fibrosis transmembrane conductance regulator (CFTR), and the elaboration of cilia on the apical surface [66-68]. Like Calu-3, the SV40 large T antigen-immortalized cell line 16HBE14o- forms tight junctions and expresses drug transporters, which makes it useful for studies of barrier function and drug transport and metabolism, but otherwise does not resemble the phenotype of a trachea-bronchial epithelial cell [68-71]. BEAS-2B, a virally-transformed, immortalized normal human bronchial epithelial cell, has found widespread use among investigators of inhalation toxicology and smoke exposure, despite uncertainty about

whether this cell line forms tight junctions [72-75]. More recently, the successful immortalization of human bronchial epithelial cells by retrovirally expressing the E6 and E7 subunits of the human papiloma virus (HPV) has been reported [76]. However, in my experience, VA10 does not differentiate into a pseudostratified epithelium when cultured at an ALI (see Appendix I). Other respiratory cell lines, such as HREC1.1, form stratified squamous epithelia when cultured under 3D conditions, and though possibly useful for the study of squamous metaplasia, it may be less helpful for the study of normal bronchial differentiation (see Appendix III). Thus, while immortalized cell lines may have desirable attributes, none have shown the differentiation capabilities of primary human bronchial epithelial cells, and therefore, cannot replace primary cells in drug metabolism, toxicology or carcinogenesis studies.

2.7 Primary Human Bronchial Epithelial Cell Culture

Methods describing the culture of airway cells date back more than 30 years [77]. In the years that followed, it was observed that airway cells became polarized and morphologically differentiated when cultured on collagen gels [78]. During this same time period, Lechner and LaVeck published their technique for isolating and culturing normal human bronchial epithelial cells using a well-defined, serum-free medium [79]. They named their medium LHC-9 [also referred to as Bronchial Epithelial Growth Medium (BEGM)], and formulated it using the Laboratory of Human Carcinogenesis (LHC) basal medium along with a plethora of supplements optimized to support the growth of human bronchial epithelial cells. This medium has become the standard medium for the isolation and expansion of human bronchial epithelium cells on cell

culture plastic ware. In 1988, Witcutt et al. described a method for culturing human bronchial epithelial cells on a gelatin membrane at an air-liquid interface, which resulted in cellular polarization and both morphological and functional differentiation [80]. Since these early studies, the media and methods for the differentiation of human bronchial epithelial cells at an air-liquid interface have been standardized, and have provided researchers with a means of reproducibly generating a well-differentiated human bronchial epithelium *in vitro* [see Table 1 for a comparison of BEGM and Air-Liquid Interface (ALI) media].

2.8 Three-Dimensional Culture Models of Human Tissues

Cells grown on two-dimensional (2D) culture surfaces cannot replicate the complexity of living tissues because the morphogenetic unit requires the presence of a morphologically and functionally specified epithelium and an intact basement membrane generated by the epithelium and the stroma. Furthermore, *in vitro* tissue recombination studies have demonstrated the importance of stroma during organogenesis. To overcome the limitations of 2D cultures, three-dimensional (3D) culture methods have been developed for a variety of tissues to replicate the cellular, structural and functional complexity observed *in situ* [81-86]. Not only do these models afford investigators an opportunity to culture cells on native matrices, such as collagens, but they allow for the co-culture of multiple cell types and the exploration of epithelial-stromal interactions *in vitro*. In addition, it has been demonstrated that cells display different phenotypes when grown on substrates of varying stiffness, and tension alone can be sufficient for the manifestation of malignant phenotype [87]. Through the alteration of substrate stiffness

by changing the concentration and/or composition of ECM proteins, or by adding cross-linking agents (see Appendix IV) or stromal cells, 3D cell culture can be used to explore tissue stiffness as a driving force of tumorigenesis and disease.

CHAPTER 3

MATERIALS AND METHODS

3.1 Cell Culture and Maintenance

IMR-90 normal lung fibroblasts (CCL-186) were purchased from American Type Culture Collection (ATCC, Manassas, VA, USA). HBECs were generously provided by Dr. Scott Randell (University of North Carolina, Chapel Hill, NC, USA). Approximately 2×10^6 first passage (P1) HBECs were expanded in 100 mm tissue culture dishes (BD Biosciences, San Jose, CA, USA) that had been pre-coated with PureCol® 100 (Advanced BioMatrix, San Diego, CA, USA). HBECs were fed bronchial epithelial growth medium (BEGM), which was prepared in accordance with published protocols (see Table 1.) [79, 88, 89]. IMR-90 and HBECs were cultured in a humidified, 37°C incubator with 5% carbon dioxide (CO_2).

3.2 LuCAF Culture and Maintenance

LuCAFs were derived from explanted lung tissues obtained from lung cancer resective surgeries. Briefly, the noncancerous margins of resected lung tissues were washed twice with sterile phosphate buffered saline (PBS) and transferred to sterile 100 mm tissue culture dishes in a biological safety cabinet. Using crossed scalpels, the tissues were minced into pieces measuring approximately 0.4 cm^3. The pieces were transferred to 35 mm tissue culture dishes (BD Biosciences) that had been pre-coated with an aqueous collagen/fibronectin/bovine serum albumin (BSA) solution. This solution contained 6 µg/ml human placental (type-IV) collagen (Sigma-Aldrich, St. Louis, MO,

USA), 1 µg/ml bovine fibronectin (Sigma), and 10.0 µg/ml BSA (Sigma). A scalpel was passed through each explanted tissue 1 – 3 times to promote adhesion to the plastic substrate. The explants were fed Dulbecco's-Modified Eagle Medium/F12 (D-MEM/F12) (Invitrogen, Carlsbad, CA, USA) supplemented with 5% fetal bovine serum (FBS) (Hyclone, Logan, UT, USA) with media changes every other day. Explants were kept in a humidified, 37°C incubator with 5% CO_2. When cells grew out from an explant, the tissue was removed once the cells reached a distance of approximately 1 cm from the original tissue border. The cells were allowed to continue proliferating until they were approximately 90% confluent, at which point they were split and given the designation passage 1 (P1). LuCAFs were routinely cultured in a humidified, 37°C incubator with 5% CO_2, and fed DMEM (Invitrogen) supplemented with 5.0% (v/v) FBS.

3.3 3D Cell Culture

Rat tail type-I collagen (BD Biosciences) was prepared according to the manufacturer's instructions and was diluted to a final concentration of 1, 2 or 3 mg/ml. Fibroblasts (IMR-90 and LuCAFs) were trypsinized during exponential growth and resuspended in type-I collagen at a concentration of 1.5×10^5 cells/ml. A total volume of 300 µl of the collagen/cell suspension was pipetted into 12 mm diameter Millicell® PICM01250 cell culture inserts (Millipore, Billerica, MA) placed within the wells of 6-well culture plates (≤ 3 inserts/well). The inserts were placed in a humidified, 37°C incubator for 15 – 30 minutes in order to promote polymerization of the collagen. Once polymerization occurred, 5 µg of human type-IV collagen was added to the apical surface of some of the collagen gels, while others remained uncoated. The type-IV collagen was

prepared by diluting a 0.5 mg/ml stock solution in F12 medium. Air-liquid interface (ALI) medium (prepared in accordance with published protocols [79, 88, 89]) was added (2 ml/well) and the gels were cultured overnight in a humidified, 37°C incubator. The following day, semi-confluent plates of HBECs were harvested with the addition of 3 ml of a 0.1 trypsin/1mM EDTA solution in PBS. Once the cells became freed from the culture vessel surface, the trypsin was inactivated by adding a sterile 2X solution of soybean trypsin inhibitor (STI) (Sigma), which was prepared by dissolving 500 mg STI into 500 ml F12 medium (Invitrogen). 1.5×10^5 viable second passage (P2) HBECs were seeded onto each collagen gel construct surface in a minimal volume of F12 medium (approximately 200 – 300 µl/insert). The cell-seeded collagen gels were returned to a humidified, 37°C incubator with 5% CO_2, and the following day, 300 µl PBS was added to each surface and aspirated in order to remove non-adherent cells and cellular debris. ALI medium was replaced every second day, and liquid on the surface of the 3D constructs was gently aspirated in order to maintain an air-liquid interface. The cell-seeded constructs were cultured at an ALI for 2 weeks in order to promote functional differentiation of the epithelium. Collagen gels containing either 1.5×10^5 HBECs or 5.0×10^4 fibroblasts served as controls. As a positive control for epithelial cell differentiation, 1.5×10^5 HBECs were seeded on 12 mm diameter Millicell® PICM01250 cell culture inserts that were pre-coated with 5 µg type-IV collagen. All experiments were performed in triplicate. See Figure 1 for a schematic of the 3D model.

Fig 1

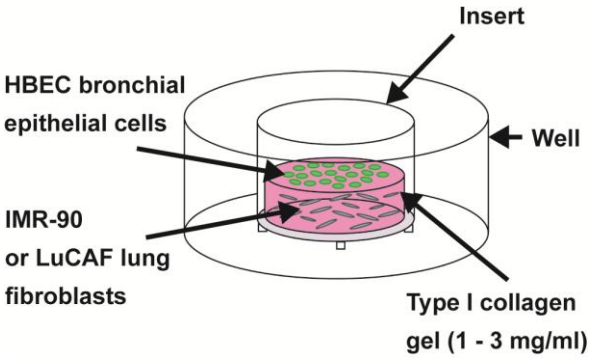

Figure 1. Schematic representation of the 3D model. HBECs are cultured on the surface, while fibroblasts are embedded within the type-I collagen gel.

Table 1. Composition of BEGM and ALI Media*

	BEGM	**ALI**
Base media:	LHC (100%)	LHC:DMEM (50:50)
Supplement	Final Conc. in Media	Final Conc. in Media
Bovine serum albumin	0.5 mg/ml	0.5 mg/ml
Bovine pituitary extract	10 µg/ml	10 µg/ml
Insulin	0.87 µM	0.87 µM
Transferrin	0.125 µM	0.125 µM
Hydrocortisone	0.1 µM	0.1 µM
Triiodothyronine	0.01 µM	0.01 µM
Epinephrine	2.7 µM	2.7 µM
Epidermal growth factor	25 ng/ml	0.5 ng/ml
Retinoic acid	5×10^{-8} M	5×10^{-8} M
Phosphorylethanolamine	0.5 µM	0.5 µM
Ethanolamine	0.5 µM	0.5 µM
Zinc sulfate	3.0 µM	3.0 µM
Penicillin G sulfate	100 U/ml	100 U/ml
Streptomycin sulfate	100 µg/ml	100 µg/ml
Gentamicin	50 µg/ml	
Amphotericin	0.25 µg/ml	
Ferrous sulfate	1.5×10^{-6} M	1.5×10^{-6} M
Magnesium chloride	6×10^{-4} M	6×10^{-4} M
Calcium chloride	1.1×10^{-4} M	1.1×10^{-4} M
Selenium	3.0 µM	3.0 µM
Manganese	0.1 µM	0.1 µM
Silicone	50 µM	50 µM
Molybdenum	0.1 µM	0.1 µM
Vanadium	0.5 µM	0.5 µM
Nickel sulfate	0.1 µM	0.1 µM
Tin	0.05 µM	0.05 µM
$CaCl_2$**	0.11 mM	1.0 mM

* Adapted from Fulcher et al.[88]

** Additional $CaCl_2$ provided by DMEM

3.4 Analysis of Collagen Gel Contraction

To determine whether increasing collagen concentrations would prevent fibroblasts and epithelial cells from contracting the collagen gels, we cast 2 mg/ml or 3 mg/ml type-I collagen gels (4-mm thickness) that were acellular or that contained either IMR-90 or LuCAFs (50,000/gel) into 12-mm Millicell™ inserts. After 7 days HBECs were added (150,000, P2) and cultured under ALI conditions for an additional 2 weeks. The inserts were observed daily using a Zeiss stereo microscope, and once contraction was observed, photographs were taken every other day using a Zeiss AxioCam HRc color CCD camera. Measurements of collagen gel contraction were made using Zeiss Axiovision version 4.4 software and calculated as the average of the longest diameter from three replicates divided by the original diameter of an uncontracted gel.

3.5 Histology and Immunohistochemistry

At harvest, the inserts were placed in 10% formalin in PBS, processed with an automatic tissue processor containing a xylene alternative (SlideBright™; American Bio-Safety, Rocklin, CA, USA), and embedded in paraffin for subsequent histological and immunohistochemical analyses. Histology stains included hematoxylin and eosin (H&E) and periodic acid Schiff with alcian blue (PAB). Primary antibodies, suppliers and working dilutions are listed in Table 2. Antibodies requiring antigen-retrieval are denoted with an asterisk. The antigen retrieval technique consisted of a microwave pretreatment in 0.01 M sodium citrate buffer (pH 6). All antigen–antibody reactions were visualized using the streptavidin–peroxidase complex with diaminobenzidine tetrahydrochloride (DAB) (Sigma). Tissues were counterstained with Mayer's hematoxylin. Tissues were

visualized and images were captured with a Zeiss Axioscope 2 Plus microscope fitted with an AxioCam HRc color CCD camera (Carl Zeiss). Epithelial thickness was determined using AxioVision software from H&E stained sections and analyzed using GraphPad Prism statistical analysis software.

Table 2. Primary antibodies for immunohistochemistry

Antigen*	Supplier	Cat. No./Clone	Specie	Dilution
Pan-keratin*	Sigma	C2562	Mouse	1:1000
Keratin 18*	Sigma	C8541	Mouse	1:100
P63*	Santa Cruz	SC-8431	Mouse	1:100
E-cadherin*	Novocastra	NCL-E-Cad	Mouse	1:75
Type I collagen*	Novus	AF5610	Mouse	1:500
Laminin V	Millipore	MAB19562	Mouse	1:200
Ki-67*	Novus	NB600-1252	Rabbit	1:100

3.6 Scanning Electron Microscopy

Harvested inserts were fixed overnight in a neutral aqueous buffer containing 2.5% glutaraldehyde and 0.1 M sodium cacodylate. The fixed gels were post-fixed in 1% osmium tetroxide followed by dehydration to 100% ethanol. The samples were critical point dried under CO_2, mounted, and sputter-coated for viewing in a scanning electron microscope.

3.7 Biomechanical Characterization of Fibroblast-Secreted Matrices

IMR-90 and primary fibroblasts were seeded onto gelatin-coated 24 mm round glass cover slips according to published protocols [90]. Briefly, fibroblasts were seeded at a density of 7.5×10^4 cells/cover slip and cultured in DMEM supplemented with 5% FBS in a humidified, 37°C incubator with 5% CO_2. When the cells on the cover slips reached 100% confluence, the growth medium was replaced with matrix medium consisting of

DMEM supplemented with 5% FBS + 50 µg/ml ascorbic acid, in order to promote the deposition of a stable ECM. The cell-seeded cover slips were fed with freshly-prepared matrix medium every second day for a period of 8 days. On day 8, the cell-seeded cover slips were harvested and analyzed with atomic force microscopy (AFM), fixed in a solution of 4% paraformaldehyde + 5% sucrose in PBS for subsequent analysis by confocal microscopy, or used for gene expression analysis.

Mechanical properties of fibroblast-derived matrices were determined using an MFP-3D atomic force microscope (Asylum Research, Santa Barbara, CA, USA). Samples were indented with a silicone nitride cantilever (manufacturer's reported spring constant = 0.06N/m) which was functionalized with a borosilicate bead (r = 10 um). The cantilever was calibrated with the thermal method prior to each experiment to determine actual spring constant. Indentation was performed in PBS at room temperature, with cantilever deflection being recorded as a function of its z-axis position. A minimum of fifteen indentations were performed per cover slip, and all measurements for a given set of samples were made on the same day. Force curves were analyzed with a custom MATLAB program which computed matrix elastic modulus using the linearized Hertz [91] model of indentation, assuming a Poisson's ratio of 0.35.

3.8 Confocal Microscopy

Confocal microscopy was performed in order to compare the thickness of ECMs secreted by IMR-90 and LuCAFs. A rabbit anti-fibronectin primary antibody (Sigma) was used at a dilution of 1:300, and a Cy2-conjugated donkey anti-rabbit secondary antibody (Jackson ImmunoResearch Laboratories, West Grove, PA, USA) was used at a

dilution of 1:500. The cover slips were counter-stained with Hoechst 33258, mounted on slides and visualized on a Zeiss LSM-510 scanning confocal microscope. ECM thickness was calculated from the Z-stack averages of 5 random locations on each cover slip.

3.9 Gene Expression Analysis

Fibroblast-seeded cover slips were harvested, total RNA was purified using an RNeasy Mini Kit (QIAGEN, Valencia, CA, USA), and the quality of the RNA was confirmed with an Agilent Bioanalyzer (Agilent Technologies, Santa Clara, CA, USA). RNA from three cover slips per sample was pooled and reverse transcribed using SuperScript® III Reverse Transcriptase (Invitrogen). Gene expression analysis was performed using Extracellular Matrix and Adhesion Molecules PCR Arrays (Cat. No. PAHS-013; SABiosciences, Frederick, MD, USA) and a MyiQ thermal cycler (Bio-Rad, Hercules, CA, USA), according to instructions provided by the manufacturers. Gene expression data was analyzed using an online software suite provided by SABiosciences. To determine whether biochemical signals from fibroblasts alter HBEC gene expression, IMR-90 or LuCAFs were seeded into 10 cm tissue culture dishes and grown in ALI medium until confluent. Conditioned media (CM) was removed from the fibroblasts, filtered through a 0.45 PVDF filter, combined 3:1 with fresh BEGM, and added to sub-confluent HBECs growing in 35 mm tissue culture dishes. The CM was replaced after 24 hours, and the cells were harvested the following day. Total RNA was isolated from the HBECs, transcribed into cDNA, and gene expression analysis was performed using Signal Transduction Pathway Finder PCR Arrays (Cat. No. PAHS-014;SABiosciences)

and analyzed for genes that were either over- or under-expressed in HBECs cultured with LuCAF CM compared to HBECs cultured with IMR-90 CM.

CHAPTER 4

RESULTS

4.1 HBECs Cultured on Millicell® Inserts

Histologic and immunohistochemical analyses revealed that HBECs cultured on Millicell® cell culture inserts generated a well-differentiated pseudostratified bronchial epithelium that contained basal, ciliated, and non-ciliated (secretory) epithelial cells when cultured at an ALI for 2 weeks (Figure 2). Tissue sections were stained with PAB to identify secreted carbohydrates (pink/purple) and glycosaminoglycans (blue), respectively. A thin layer of glycoconjugates was apparent along the apical surface of the tissues (Figure 2B, *black arrow)*, confirming both the presence of secretory epithelial cells and that the tissues were functionally specialized. These cells secreted a

Fig 2

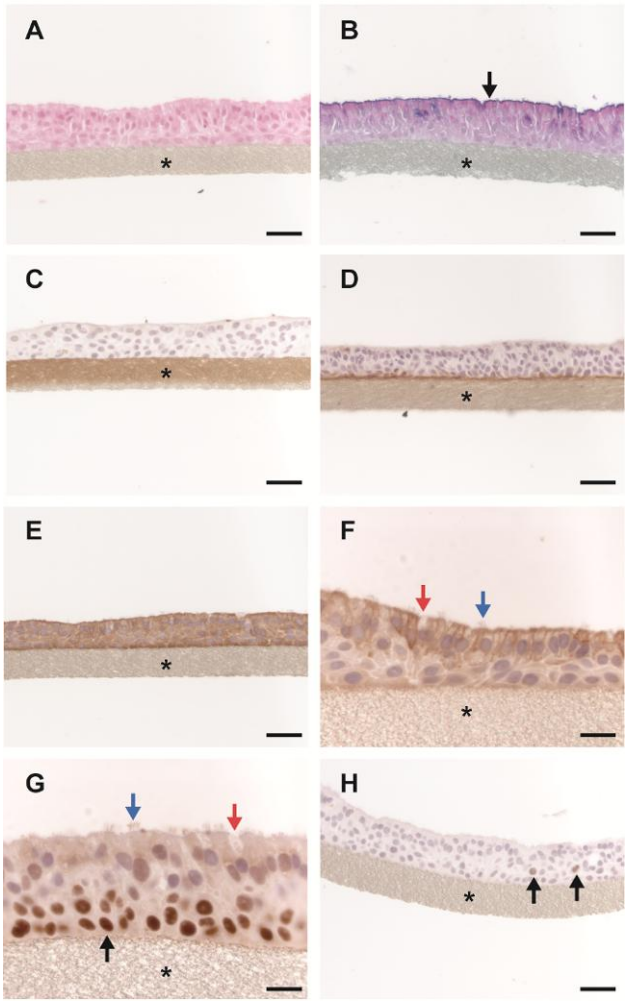

Figure 2. Characterization of HBECs cultured on type-IV collagen coated 12-mm Millicell™ inserts. HBECs (150,000/insert) were cultured for 2-wk at the air-liquid interface and paraffin-embedded tissues were sectioned and analyzed by staining with H&E (2A), PAB (2B), or immunostained with antibodies against col IV (2C), lam 5 (2D), Pan-K (2E), K18 (2F), P63 (2G), and Ki-67 (2H). The type-IV collagen coated filter insert is marked with an asterisk (*). Secretory goblet cells are marked with red arrows (2F – 2G). Ciliated columnar epithelial cells are marked with blue arrows (2F – 2G). Ki-67 positive nuclei are marked with black arrows (2H). Scale bars represent 16 µm (2F – 2G) and 40 µm (2A – 2E, 2H).

basement membrane positioned between the collagen type-IV coated filter (Figure 2C) and the epithelium, as evidenced by positive staining for laminin 5 (Figure 2D). Immunostaining for keratins confirmed that they were epithelial (Figure 2E). Staining with a keratin 18 antibody demonstrated that the columnar epithelial cells were at the apical surface (Figure 2F). P63-positive basal epithelial cells were evident along the basal surface of the tissues (2G, *black arrow*). The pseudostratified columnar epithelium consisted of both ciliated (Figure 2F and 2G, *blue arrows*) and non ciliated (secretory) epithelial cells (Figure 2F and 2G, *red arrows*, and Figure 4A – 4B). Immunostaining with an anti-Ki-67 antibody showed that very few cells per field were proliferating at the 2-wk time point. (Figure 2H, *arrows*).

4.2 HBECs Cultured on 1 mg/ml Collagen Gels

To determine whether HBECs cultured on thick collagen matrices grew similarly to HBECs grown on coated Millicell™ inserts, and whether type-IV collagen was required for cell attachment, HBECs (150,000, P2) were seeded onto either 1 mg/ml type-I collagen gels or 1 mg/ml type-I collagen gels coated with 5 µg type-IV collagen (referred to as "type-IV on I") that had been cast into 12-mm Millicell™ inserts. At the two week time point, the epithelial cells were organized in a stratified manner compared to HBECs cultured on type-IV collagen coated Millicell™ inserts (Figure 3A – 3B). Keratin staining revealed that the cells maintained an epithelial phenotype (3C – 3D). Most notably, the columnar cells stained less robustly for keratin 18 (Figure 3E – 3F), and the P63 staining pattern was less orderly (Figure 3G – 3H). In some areas, basal cells lost nuclear P63 expression (*red arrows*), and in others, P63 was expressed in multiple

cell layers (*blue arrows*). The epithelium appeared thicker on Type-IV on I gels than Type-I gels. Ultrastructural analysis demonstrated the presence of cilia on HBECs cultured on either collagen gel type (Figure 4).

Fig 3

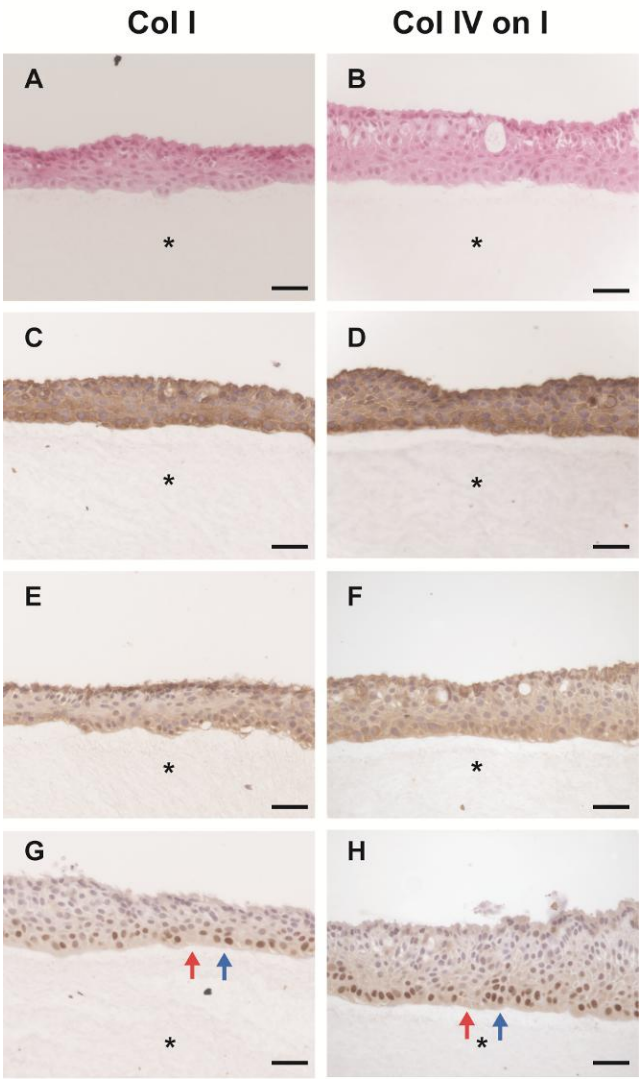

Figure 3. Characterization of HBECs cultured on 1mg/ml type I collagen gels. HBECs were cultured on 1 mg/ml type I collagen gels (3A, 3C, 3E, 3G) or 1 mg/ml type I collagen gels coated with 5 µg type-IV collagen (3B, 3D, 3F, 3H). HBECs (150,000/gel) were cultured for 2-wk at the air-liquid interface and paraffin-embedded tissues were sectioned and analyzed by staining with H&E (3A – 3B) or immunostaining with antibodies against Pan-K (3C – 3D), K18 (3E – 3F), or P63 (3G – 3H). The type-IV collagen coated filter insert is marked with an asterisk (*). Ki-67 negative basal cells are marked with red arrows (3G – 3H), and Ki-67 basal cells are marked with blue arrows (2F – 2H). Scale bars represent 40 µm.

Fig 4

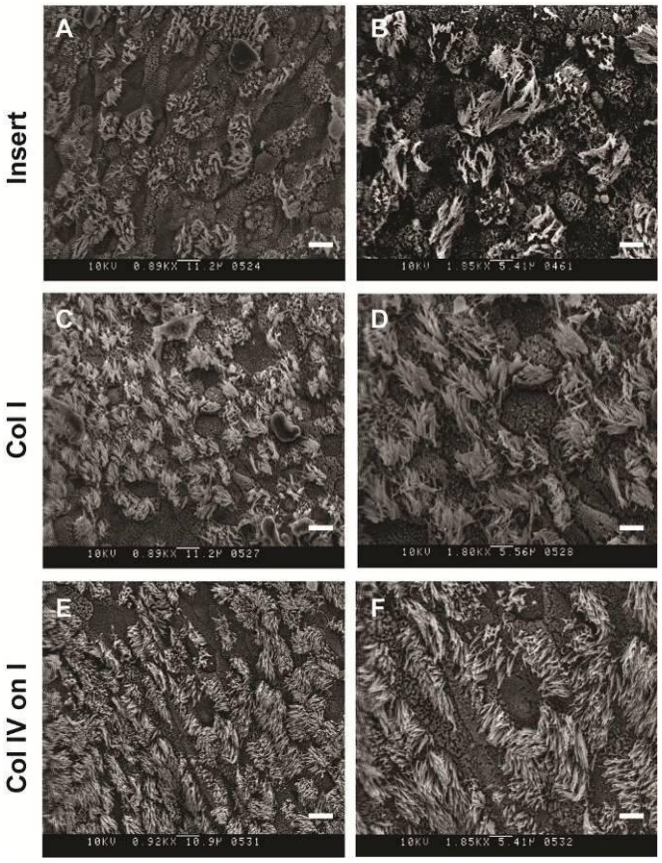

Figure 4. Scanning electron micrographs of HBECs cultured on type-IV coated Millicell™ inserts (4A – 4B), 1 mg/ ml type I collagen gels (4C – 4D), or 1 mg/ ml type I collagen gels coated with 5 µg type-IV collagen (4E – 4F). Ciliated epithelial cells are present under all conditions. Scale bars represent 5.41 µm (4B, 4F), 5.56 µm (4D), 10.9 µm (4E), or 11.2 µm (4A, 4C).

4.3 Effect of LuCAFs on HBECs in 1 mg/ml Collagen Gels

HBECs cultured on collagen gels showed a dramatically different phenotype depending on whether they were grown on collagen gels that contained LuCAFs or IMR-90 fibroblasts. Specifically, LuCAFs facilitated HBECs to invade the collagen matrix, while IMR-90 promoted HBECs to form a surface epithelium (Figure 5A, 5C, 5E, 5G). HBECs in gels containing LuCAFs formed both hollow (Figure 5B, *blue arrow*) and solid structures (Figure 5B, *red arrow*). These structures were made up of epithelial cells (Figure 5H), some of which expressed the cell-cell adhesion protein E-cadherin (Figure 6B). In some instances, cells that formed hollow structures were E-cadherin-positive

(Figure 6A – 6B, *blue arrows*), while those adjacent to these structures were negative (Figure 6A – 6B, *red arrows*). Both the hollow and the solid structures were polarized, as evidenced by P63-positive cells along the outermost perimeter (Figure 6C - 6D). In addition, the cells forming these structures deposited large amounts of the basement membrane protein laminin 5 (Figure 5G – 5H).

Fig 5

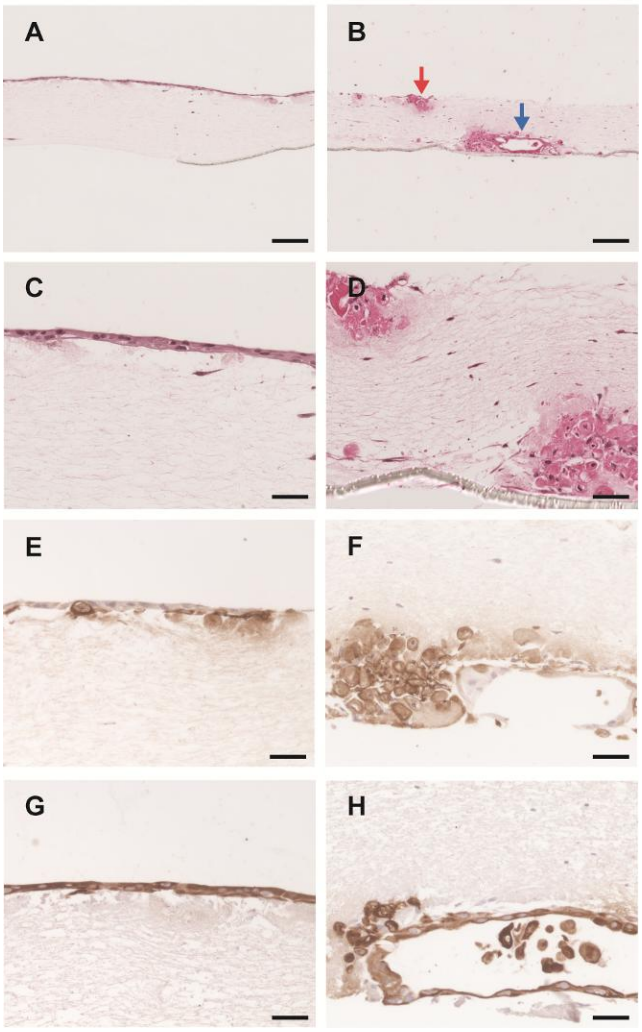

Figure 5. Characterization of HBECs cultured on 1mg/ml type I collagen gels containing fibroblasts. HBECs (150,000/gel) and fibroblasts (50,000/gel)were co-cultured for 2-wk at the air-liquid interface and paraffin-embedded tissues were sectioned and analyzed by staining with H&E (5A – 5D) or immunostaining with antibodies against Lam 5 (5E – 5F) and Pan-K (5G – 5H). Gels contained either IMR-90 fibroblasts (5A, 5C, 5E, 5G) or LuCAFs (5B, 5D, 5F, 5G). Red and blue arrows identify solid and hollow epithelial structures, respectively (5B). Scale solid bars represent 40 µm (5B, 5D, 5F, 5G) and 160 µm (5A, 5C, 5E, 5G).

Fig 6

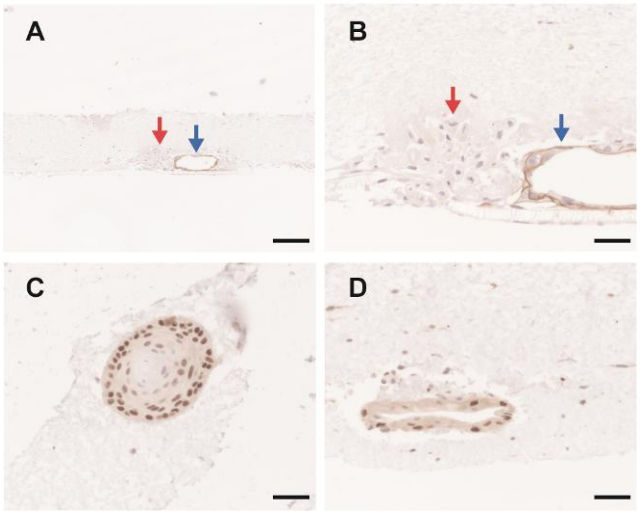

Figure 6. Characterization of solid and hollow epithelial structures observed in type I collagen gels that contained LuCAFs. HBECs (150,000/gel) and LuCAFs (50,000/gel) were co-cultured for 2-wk at the air-liquid interface and paraffin-embedded tissues were sectioned and analyzed by immunostaining with antibodies against E-cad (6A – 6B) and P63 (6C – 6D). Red and blue arrows identify solid and hollow epithelial structures, respectively (6A – 6B). Scale solid bars represent 40 µm (6B – 6D) and 160 µm (6A).

4.4 Effect of LuCAFs on HBECs in 3 mg/ml Collagen Gels

The 1 mg/ml collagen gels were heavily contracted by fibroblasts and epithelial cells. LuCAFs contracted 1 mg/mI type-I collagen gels more than IMR-90 fibroblasts, and HBECs alone were able to contract the collagen gels to a lesser extent (data not shown). We hypothesized that increased concentrations of collagen would prevent this cell-mediated contraction. By culture day 13 (day 6 after seeding epithelial cells), the 2 mg/ml collagen gels containing HBECs were more contracted than gels that contained fibroblasts alone (Figure 7A and 7B). While the combination of HBEC and LuCAFs resulted in more contraction than the combination of HBEC and IMR-90 in the 2 mg/ml collagen gels, the 3 mg/ml gels reduced contraction in all gels (Figure 7A and 7B). Maximal contraction occurred by culture day 13, and no additional contraction was observed subsequently.

To determine the effect of collagen concentrations (2 mg/ml or 3 mg/ml) on the HBEC phenotype, HBECs were seeded on acellular collagen gels or collagen gels that

contained either IMR-90 or LuCAFs. HBECs generated a pseudostratified epithelium when cultured on either 2 mg/ml or 3 mg/ml collagen gels (Figure 8A – 8B). These epithelia contained basal, goblet and ciliated epithelial cells (data not shown). There was no difference in the thickness of the epithelium in either the 2 mg/ml or 3 mg/ml collagen gels (Mann Whitney test, P = 0.700, N = 10) (Figure 9A) but the epithelium was significantly thicker in gels that contained either IMR-90 or LuCAFs (one-way analysis of variance [ANOVA], P < 0.0001, N = 20) (Figure 9B). In addition, these data suggested that gels that contained LuCAFs have a thicker epithelium than the gels that contain IMR-90 (Figure 9B). In collagen gels that contained LuCAFs, nodular epithelial structures could be observed beneath the surface epithelium in the 2 mg/ml collagen gels (Figure 8E). These structures were not observed in the 3 mg/ml collagen gel containing LuCAFs (Figure 8F), or in any of the other conditions (8A – 8D).

Fig 7

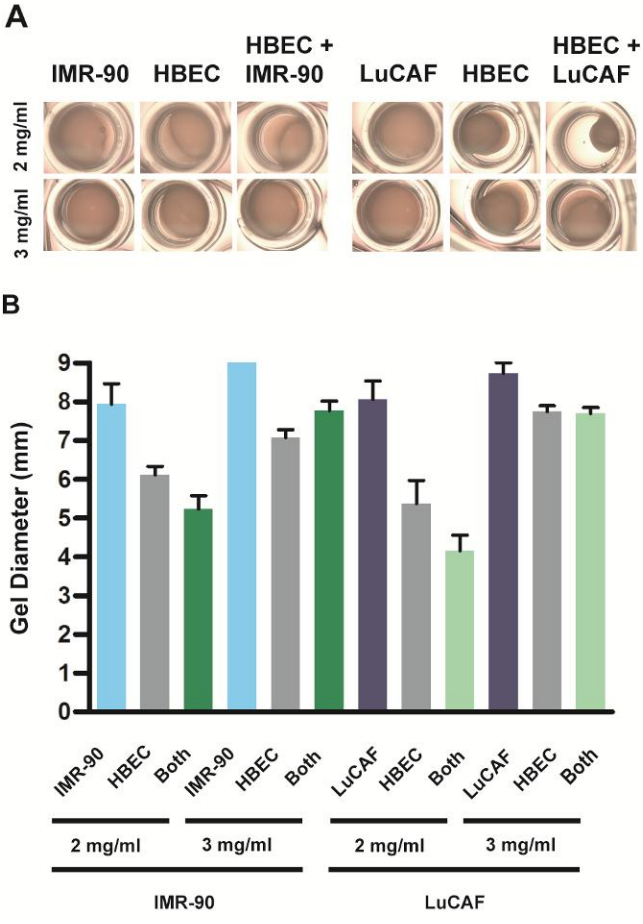

Figure 7. Analysis of contraction in 2 mg/ml and 3 mg/ml type I collagen gels. Gels were seeded with fibroblasts (IMR-90 or LuCAF), HBECs, or fibroblasts and HBECs. Maximal contraction was observed on culture day 13. HBECs contracted both 2 mg/ml and 3 mg/ml more than either IMR-90 or LuCAF, which did not differ in their ability to contract the collagen gels. HBECs co-cultured with LuCAF contracted collagen more than cultures that contained HBECs alone, fibroblasts alone, or HBECs co-cultured with IMR-90.

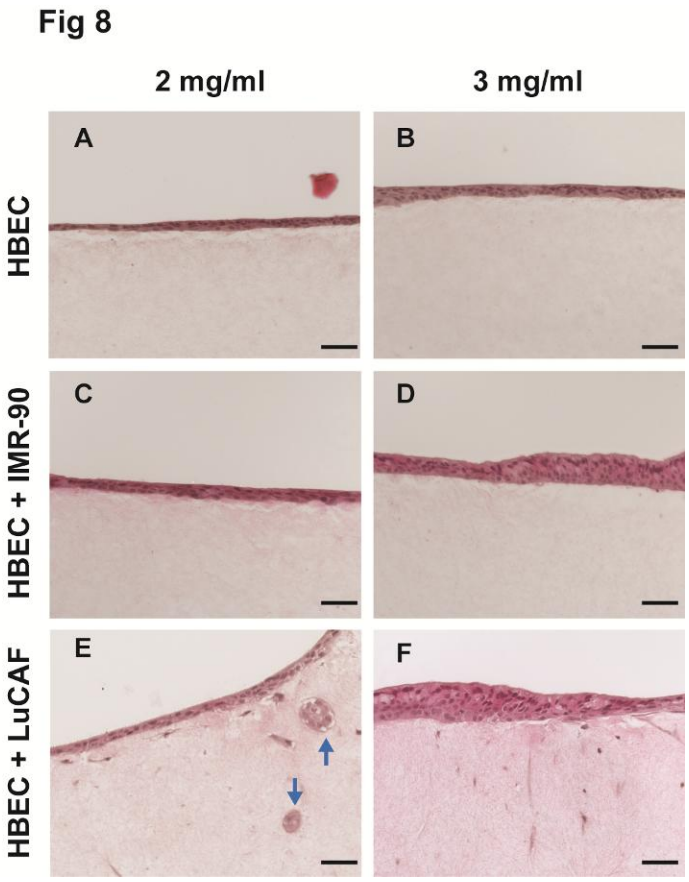

Figure 8. Characterization of HBECs cultured on 2 mg/ml and 3 mg/ml type I collagen gels. Gels containing HBECs (150,000/gel) (8A – 8B), HBECs (150,000/gel) and IMR-90 (50,000/gel) (8C – 8D), or HBECs (150,000/gel) and LuCAFs (50,000/gel) (8E – 8F) were cultured for 2-wk at the air-liquid interface and paraffin-embedded tissues were sectioned and analyzed by staining with H&E (8A – 8F). Blue arrows indicate solid epithelial structures within the collagen gel. Scale solid bars represent 40 µm.

4.5 Analysis of ECM Stiffness

To determine whether IMR-90 and LuCAFs secrete matrices of comparable thickness and stiffness, the fibroblasts were cultured under conditions that promoted ECM deposition, and the fibroblast secreted ECMs were analyzed by confocal and atomic force microscopy. IMR-90 and LuCAFs secreted fibronectin-rich matrices of comparable thickness (13 µm vs. 11 µm, respectively) (Figure 10A.) However, atomic force microscopy revealed that the matrices secreted by LuCAFs were more than twice as stiff as the matrices secreted by the IMR-90 fibroblasts (Figure 10B).

Fig 9

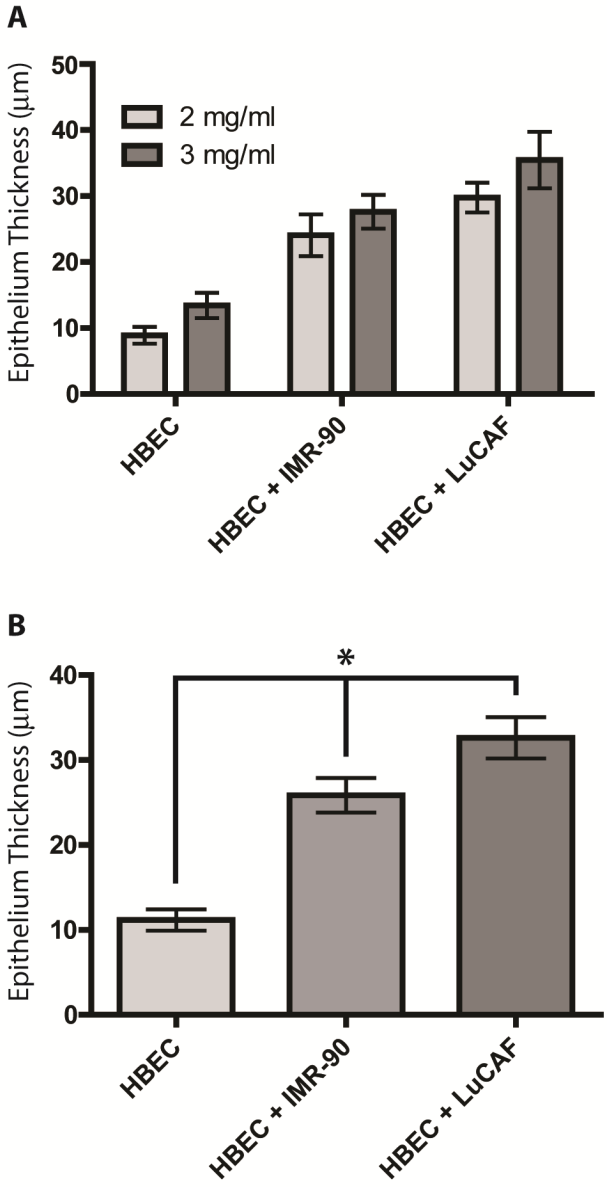

Figure 9. Measurement and analysis of epithelial thickness in type-I collagen gels. Type-I collagen gels (2 mg/ml or 3 mg/ml) were cast into Millicell culture inserts either without fibroblasts or with IMR-90 or LuCAFs. 150,000 HBECs were seeded on the surface and cultured for an additional 2 weeks at an ALI. Tissue thickness was determined using AxioVision software from H&E stained sections and analyzed using GraphPad Prism statistical analysis software. No difference was observed between the 2 mg/ml and 3 mg/ml gels (9A, Mann Whitney test, $P = 0.700$, $N = 10$). However, gels that contained fibroblasts were statistically thicker than gels that lacked fibroblasts (9B, one-way analysis of variance, $P < 0.0001$, $N = 20$).

4.6 Gene Expression Analysis of Fibroblasts and HBECs

To determine whether the observed stiffness was due to an up-regulation of ECM genes, Q-PCR was performed using Extracellular Matrix and Adhesion Molecules (PAHS-013) 96-well Q-PCR Arrays (SABiosciences). None of the major ECM collagens were up-regulated or down-regulated (Table 3). However, changes were evident in

several matrix metalloproteinase genes, indicating that the major difference between IMR-90 and LuCAFs may be in how they modify their ECMs.

To determine whether biochemical mediators may be involved in determining the HBEC phenotypes, HBECs were cultured in BEGM preconditioned by either IMR-90 or LuCAFs. An equal and controlled amount of reverse-transcribed cDNA was run on Signal Transduction Pathway Finder (PAHS-014) 96-well Q-PCR arrays (SABiosciences) and analyzed for genes that were either over- or under-expressed in HBECs cultured with LuCAF CM compared to HBECs cultured with IMR-90 CM. Only 6 genes were more than two-fold under- or over-expressed (Table 4). Over-expressed genes were Chemokine (C-X-C motif) ligand 9 (CXCL), FAS ligand (FASLG), and telomerase reverse transcriptase (TERT). Under-expressed genes were baculoviral IAP repeat-containing 2 (BIRC2), Kallikrein-related peptidase 2 (KLK2), and early growth response 1 (EGR1).

Fig 10

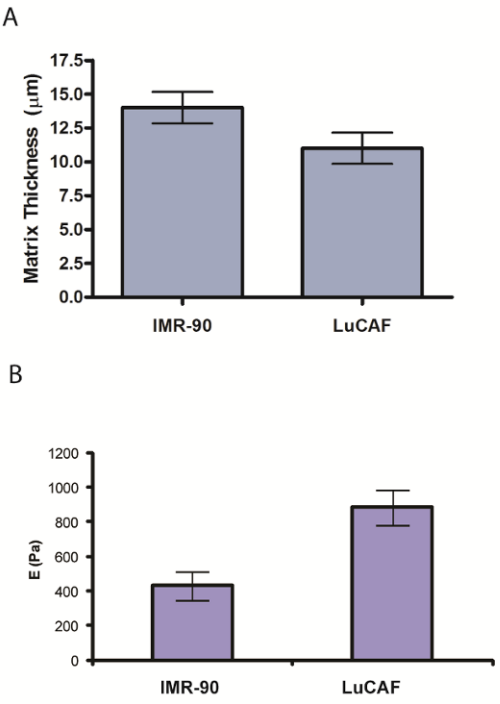

Figure 10. Biomechanical analysis of fibroblast secreted matrices. Fibroblasts were seeded on glass cover slips under conditions that promoted the deposition of stable ECMs. The thickness of the ECMs was determined by confocal microscopy with an antibody that recognizes fibronectin (9A). There was no difference in the observed thickness matrices secreted by either IMR-90 or LuCAFs (N = 5, P = 0.076, two-tailed t-test. The stiffness of the matrices was determined by atomic force microscopy (9B). Matrices secreted by LuCAFs were more than two-fold stiffer than matrices secreted by IMR-90 fibroblasts (N = 3, P = 0.013 one-tailed t-test, P = 0.025, two-tailed t-test).

Table 3. Genes up-regulated in LuCAF vs. IMR-90 (Control)	
Gene	Up / Down
ADAMTS8	+10.12
ITGA7	+11.32
ITGB2	+7.71
LAMA3	+9.13
MMP12	+6.01
MMP3	+15.62
NCAM1	+7.84
THBS2	+7.21
CLEC3B	+5.63
COL15A1	-6.04
MMP11	-6.28
MMP16	-20.64
MMP8	-4.79

Table 4. Genes up- or down-regulated in HBECs fed LuCAF CM vs. IMR-90 CM (Control)	
Gene	Up / Down
CXCL9	+4.12
FASLG	+3.12
TERT	+3.12
BIRC2	-2.23
KLK2	-2.22
EGR1	-2.07

CHAPTER 5

DISCUSSION

Biophysical and biochemical interactions between the stroma and epithelium regulate normal lung development, as well as lung homeostasis and the initiation and progression of lung pathologies such as cancer [50, 92, 93]. Lung cancer is the leading cause of cancer deaths worldwide, and lung cancer death rates in the United States have remained nearly unchanged for three decades[94]. In part, this is due to the fact that public policy aimed at reducing tobacco consumption has failed.

Because mice and rats fail to develop lung cancer when exposed to cigarette smoke, human surrogate models have been used to observe how toxicants affect the human lung tissues. Established human bronchial epithelial cell lines, such as Calu-3 and 16HBE14o-, have been cultured at an air-liquid interface in order to generate representative models of the human bronchial epithelium for use in toxicological and drug transport studies [95, 96]. However, these cultures do not mimic the bronchial epithelium in either form or function. To overcome this limitation, methods have been described for differentiating primary human bronchial epithelial cells at an air-liquid interface [88, 89].

Though primary bronchial epithelial cells form morphologically correct and functional epithelia when grown under these conditions, their scarcity has led some to develop immortalization methods as an attempt to generate a more abundant supply of cells [76, 87, 97]. Unfortunately, these cells have either not been disseminated throughout the research community, or in the case of VA10, we found that they did not form

pseudostratified ciliated epithelia when cultured at an air-liquid interface, as the authors claimed (see Appendix I). It is possible and likely that transfection and/or infection with viruses has a significant impact on cellular phenotypes. This is inferred from the fact that when expressed in osteosarcoma cells, the seemingly innocuous reporter gene green fluorescent protein (GFP) increased the aggressiveness of these tumorigenic cells *in vivo* [98].

To overcome the many limitations of conventional 2D cell culture, we have employed 3D cell culture as a means of creating morphologically correct and functional tissues with which to study epithelial-mesenchymal interactions in the homeostatic maintenance and pathogenesis of human tissues. The establishment of a comprehensive 3D model of the bronchial mucosa containing bronchial stroma and epithelial tissue represents a significant challenge because of the technical difficulties in obtaining abundant cells from both normal and pathological sources. Overcoming these shortcomings will allow for a systematic analysis and synthesis of the normal and pathological interactions among the constituent layers of the bronchial tree. Our data stemming from the exploration of a 3D bronchial multi-tissue model suggest that co-cultures of human bronchial epithelial cells with primary lung fibroblasts can be a valuable tool to help researchers in understanding how epithelial and stromal interactions regulate lung homeostasis and disease.

We have reported that HBECs formed a well-differentiated pseudostratified columnar epithelium when cultured for two weeks at an ALI. These epithelia contained: p63-positive basal epithelial cells, K18-positive columnar epithelial cells, and secretory goblet cells, as evidenced by positive staining with PAB; and non-secretory ciliated

epithelial cells, which were evident in phase contrast microscopy, scanning electron micrographs and histological sections. In addition, positive immunostaining for keratin-5 confirmed the presence of a basement membrane; while Ki-67 immunostaining revealed that very few epithelial cells within these tissues were undergoing proliferation at the two-week time point. While these cultures replicated many of the morphological and functional characteristics of the human bronchial epithelium, they lacked a stroma, and therefore the full complexity of bronchi *in situ*.

In order to study how components of the lung stroma, such as fibroblasts and extracellular matrix proteins, affected the phenotype of the bronchial epithelium, we increased the complexity of our ALI cultures by adding normal lung fibroblasts (IMR90) and lung cancer-associated fibroblasts (LuCAFs) embedded within a type-I collagen matrix to mimic the bronchial lamina propria. Type-I collagen is the most abundant structural protein in mammalian lungs, and it has become a popular biomaterial for tissue engineering and 3D cell culture due to the fact that it is biocompatible, biodegradable, and readily forms gels at concentrations as low as 0.125% w/v [99]. Type-I collagen is commercially available from several sources and the purity and composition of these products have been characterized [100]. There have been several previous reports describing the co-culture of lung fibroblasts and human bronchial epithelial cells in 3D type-I collagen gels [43, 81, 101, 102]. However, these published models used collagen concentrations that varied widely from 0.715 mg/ml to 2.5 mg/ml, which generated varied results.

Our data show that collagen concentration and composition affected the phenotype of bronchial epithelial cells in 3D culture. On the 1 mg/ml type-I collagen

gels, epithelia became stratified compared to HBECs that were cultured on coated Millicell™ inserts. In addition, the columnar cells stained less robustly for keratin 18 and the P63 staining pattern was less orderly. The addition of type-IV collagen generated epithelia that were thicker than when the gels consisted of type-I collagen alone. This could be a result of basal epithelial cells adhering more robustly to the type-IV collagen, which is a component of basement membranes. These results confirm that HBECs grew on thick collagen matrices, and that HBECs adhered to both type-I and type-IV collagen, but under these conditions the epithelium did not differentiate optimally.

HBECs cultured on 1 mg/ml collagen gels that contained LuCAFs showed a dramatically different phenotype than when cultured on 1 mg/ml collagen gels that contained IMR-90 fibroblasts. Specifically, LuCAFs seemed to facilitate HBECs to invade the collagen matrix, while IMR-90 promoted HBECs to form a surface epithelium. Within the collagen gels that contained LuCAFs, we observed solid nodular epithelial structures and hollow cyst-like epithelial structures. Interestingly, these structures had regions that were stained differentially positive and negative for the cell-cell adhesion protein E-cadherin.

All of the type-I collagen gels were contracted, regardless of whether they contained epithelial cells, fibroblasts, or co-cultures of the two cell types. However, LuCAFs and co-cultures of LuCAFs and HBECs caused more contraction than IMR-90 or co-cultures of IMR-90 and HBECs. Type-I collagen gels can be contracted by several cell types, including lung fibroblasts and epithelial cells, and the extent of contraction is reportedly increased when the two cell types were combined in co-culture [103-105]. We

suspect that invasive HBEC phenotype could be due to HBECs and fibroblasts contracting the type-I collagen gels.

To understand how physical forces from the contracting collagen gels could alter the phenotype of HBECs, one should consider the types of forces to which the bronchus and the bronchial epithelium are typically exposed. Under normal breathing conditions, the intra-luminal air pressure varies by approximately 1 cmH_20, and therefore, the circumference of the bronchus does not change significantly [106]. In unobstructed airways, bronchial epithelial cells are exposed to pressures of approximately 1 cmH_20 (98 Pa), and as a result, airway cells are in a state of physical homeostasis. Compressive stress (pressure that is directed perpendicularly against a surface) occurs when the bronchus constricts and buckles, thus forcing apical surfaces of neighboring cells against one another. In a constricted airway, pressure from compressive stress can exceed 30 cmH_20 (2.9 KPa) [107, 108].

Using air-liquid interface cultures of bronchial epithelial cells, Ressler demonstrated that compression alone could cause airway fibrosis independent of inflammation through an activation of pro-fibrotic genes, including early growth response protein 1 (EGR-1) [109]. In endothelial cells, EGR-1 is activated by mechanical force and vascular injury. EGR-1 activates the transcription of platelet-derived growth factor (PDGF), which is an activator of collagen production in fibroblasts [110-112]. In addition, the transforming growth factor beta 1 (TGF-β1) gene promoter has a binding site for the transcription factor EGR-1, and TGF-β1 has been shown to stimulate type-I collagen production by fibroblasts. Interestingly, we demonstrated that HBECs up-regulated EGR-1 when exposed to conditioned medium from LuCAFs but not IMR-90.

These data support Ressler's finding that bronchial fibrosis can be mediated by both biomechanical and biochemical means.

Previous reports described fabricated tissue anchors as a means of inhibiting the contraction of collagen gels [81, 101]. I was unable to prevent collagen gel contraction using these published protocols (data not shown). I infer that the reason why I observed contraction when others did not is that my experiments were seeded with low passage HBECs ($\leq 3^{rd}$ passage; ≤ 6 population doublings). It is evident from the materials and methods section of some published reports that investigators may plate their primary HBECs sparsely in an attempt to produce a larger number of cells for their experiments. As a result, these cells may be low passage but they have doubled more than six times; we have observed that the HBEC phenotype changes beyond the 6^{th} population doubling, including a loss of contractility and the ability to differentiate at an ALI.

Enzymatic collagen cross-linkers, such as lysyl oxidase (LOX) and tissue transglutaminase (TGase), have been proposed as an effective and non-cytotoxic means of inhibiting collagen gel contraction [113-115]. Unfortunately, lysyl oxidase was not available from commercial sources during the time period of this dissertation, and our experiments with tissue transglutaminase cast doubt on whether it truly cross-links commercially obtained type-I collagen (see Appendix V).

In addition to chemical cross-linkers, we explored whether peptide hydrogels and silk fibroin scaffolds could be useful for the construction of a 3D model of the human bronchus, since these materials would likely not be contracted by cells due to their molecular composition. In our hands, HBECs failed to adhere to and/or grow on either of these matrices (see Appendix VI), but we prefer not to make definitive conclusions from

these experiments due to the fact that our results from these pilot studies constitutes a very small sample.

While our data are consistent with reports that describe cell-mediated contraction of collagen gels, we found that increased concentrations of collagen alone were sufficient to minimize contraction. Furthermore, we observed that co-cultures of LuCAFs and HBECs contracted 2 mg/ml type-I collagen gels to a greater extent than co-cultures of IMR-90 and HBECs. IMR-90 and LuCAFs contracted collagen gels to a similar extent, suggesting that the greater contraction observed in co-cultures of LuCAFs and HBECs may have been due to reciprocal communications between the two cell types. Furthermore, in the 2mg/ml and 3mg/ml gels, there was a significant positive correlation between collagen concentration and/or the inclusion of fibroblasts and epithelium thickness. These altered phenotypes might have been due to different physical forces affecting HBECs when cultured on the collagen gels compared to the Millicell™ cell culture inserts.

To determine whether in our multi-cellular model lung fibroblasts altered the phenotype of HBECs through modification of the extracellular matrix (ECM), we compared the deposition of extracellular matrix by normal and tumor-associated fibroblasts. IMR-90 and LuCAFs fibroblasts secreted fibronectin-rich matrices of comparable thickness (13 μm vs. 11 μm, respectively). However, the matrices secreted by the LuCAFs were more than twice as stiff as the matrices secreted by the IMR-90 fibroblasts. Therefore, differences in the biomechanical properties of a normal stroma and a stroma derived from tumor-associated fibroblasts may contribute to the disruption of bronchial tissue homeostasis.

To determine whether these phenotypes were due to secreted biochemical mediators, we cultured HBECs in bronchial epithelial growth medium preconditioned by either IMR-90 or LuCAFs. Only 6 genes were more than two-fold under- or over-expressed (See Table 4). Those six genes are associated with immune responses, apoptosis, mitosis, cell survival, and differentiation. TERT has been shown to be up-regulated in solid tumors of the lung [116]. Dysregulation of CXCL9 and its receptor, CXCR3, have been associated with pulmonary inflammation [117-120]. The KLK family of peptidases have been explored for their utility as biomarkers for a variety of cancers [121]. EGR1 dysregulation in pulmonary tissues has been associated with both acute lung injury and exposure to cigarette smoke. More recently, a loss of EGR1 expression has been linked to a subsequent increase in CXCL9 expression in murine Lewis lung carcinoma (LLC1) xenografts [122]. The structural (histological) and clinical significance of these findings awaits confirmation by others.

In conclusion, we have created a functionally and morphologically representative 3D multi-cellular model of the human bronchial mucosa. We have used this model to study how cellular and acellular components of the bronchial stroma affect the phenotype of the bronchial epithelium. Additionally, we found that LuCAFs had a clear effect on epithelial organization, suggesting that, like in other organs, the stroma is a main determinant of neoplastic development.

We anticipate that this model will be of value for the study of inhaled toxicants and carcinogens, drug transport and metabolism, and bronchial homeostasis and pathogenesis. Our studies highlighted the critical importance of matrix composition and concentration, and identified variables that must be optimized (i.e. type-I collagen

concentration and prevention of collagen gel contraction) and pitfalls that should be avoided (i.e. over-passaging of HBECs). As 3D models are adopted by more researchers, additional information will be generated that will allow investigators to increase their complexity through the inclusion of additional cell types, such as endothelial, smooth muscle, or immune cells. These models will provide researchers with a more accurate representation of living human tissues and a more efficient use of the limited funds for scientific research.

CHAPTER 6

FUTURE DIRECTIONS

I learned a great deal from my thesis studies, and I am grateful to all of my teachers for their lessons. To those who will read this thesis, I sincerely hope that my results will inform and inspire, and guide them in their desire to work with 3D cell culture models. By now, it should be evident that 3D cultures are necessary if we wish to understand complex biological systems and draw accurate conclusions from our experiments. However, be forewarned that by adding another dimension (i.e. 3D matrices) to cell culture, we are introducing many additional variables that must be acknowledged, understood, and in some cases rigorously controlled. The sooner one identifies all the variables in their culture system, the sooner they can begin to extract meaningful data from their experiments.

In many ways, type-I collagen is the ideal biomatrix for the 3D culture of human bronchial epithelial cells. It is the most abundant structural collagen of the submucosa, it is commercially available in (somewhat) purified form, it is relatively easy to work with, stromal cells can be incorporated into an unpolymerized buffered collagen solution, and HBECs adhere to and proliferate on type-I collagen. Collagen polymerization is affected by its pH, the age (shelf-life) of the collagen stock solution, the temperature of the collagen solution, and atmospheric gas composition. Therefore, care must be taken to standardize these parameters in order to assure that gels polymerize similarly each time, and therefore have similar biomechanical/viscoelastic properties. Rheometers,

microindentors, and atomic force microscopes can be used to accurately assess the mechanical properties of collagen gels.

In my experience, the biggest challenge in working with collagen gels is that cells contract collagen. Under normal breathing, the bronchial epithelium exists in a state of mechanical homeostasis, and only experiences stress/strain under constrictive conditions. Therefore, contraction must be prevented in order to mimic the homeostatic bronchus. We were able to minimize contraction by increasing the concentration of type-I collagen from 1mg/ml to 3 mg/ml. However, one should consider the effect that high concentrations of collagen have upon the cells of one's culture system. High collagen concentrations may produce gels that are stiffer than the tissue(s) that one is trying to mimic, and it has been demonstrated that substrate stiffness regulates the phenotype of cells. In addition, high concentrations of collagen may hinder the transport of macromolecules to the cells.

Enzymatic collagen cross-linkers could be incorporated into collagen gels in order to prevent cell-mediated contraction. Lysyl oxidase appears to be the most promising collagen cross-linking agent. Unfortunately, lysyl oxidase is not readily available from commercial sources, but its utility should be explored if an adequate supply can be secured. Non-enzymatic cross-linkers, such as ultraviolet light, could be investigated if methods could be developed to incorporate stromal cells into the gel post-cross-linking. Alternatively, other types of collagen-based matrices could be utilized, such as electrospun collagen mats. Finally, synthetic and natural matrices, such as peptide hydrogels and silk-based scaffolds, should be thoroughly evaluated.

Alternatively, we demonstrated that pulmonary fibroblasts are capable of secreting matrices when fed growth medium supplemented with ascorbic acid. One could consider allowing fibroblasts to secrete a native matrix upon which HBECs would be seeded and differentiated. This method may offer several advantages over other more defined matrices. Fibroblasts can be easily removed from their ECMs using a mild basic solution of sodium hypochlorite. This can be utilized to generate acellular matrixes in order to study the differential effects that stromal cells and ECM have upon epithelial cells. We demonstrated that gene expression analysis can be performed on fibroblasts within secreted matrices. Likewise, it is technically feasible to remove the bronchial epithelium using a mild enzyme, such as dispase, in order to perform similar expression analyses. We demonstrated that biomechanical analyses can be performed on the fibroblast-secreted matrices, and multiphoton microscopy could be employed to understand how collagen fiber length, diameter and orientation combine to influence the phenotype of bronchial epithelial cells.

Once an ideal matrix has been identified, the phenotypic readout of the epithelium should be considered. We utilized numerous techniques, such as histology, immunohistochemistry, light microscopy, confocal microscopy, electron microscopy, atomic force microscopy, and quantitiative gene expression analysis. Other forms of analysis may be equally informative as the ones we used. Rheometry could be used to study both the biomechanical properties of the tissue and the viscosity of secreted mucins. Fluorescent microbeads could be used along with fluorescent time-lapse microscopy to study ciliary beat and mucus clearance. Proteomics could be used to identify proteins secreted by cells of the 3D system in response to injury, drugs, and/or

toxicants. When technically possible, cinematography could provide an illustration of how motion is altered (restricted or facilitated) under given experimental conditions that mimic "real life" conditions.

The examples I mentioned above will undoubtedly expand as more people abandon the limits of 2D cell culture in favor of modular and tunable 3D cell culture models. Additional matrices and ECM products will become available in the near future, and human primary cells from healthy and diseased tissues can now be purchased from multiple commercial sources. When these are combined in the right manner, we can finally begin to address more challenging biological questions.

In its infancy, 3D culture techniques were used by a small number of labs to explore rather narrow technological and basic research questions. With the sizable expansion of labs interested in these applied and strictly research-oriented topics, the specific aims and expectations have multiplied almost exponentially. However, one stumbling block in this process has been a lack of standardization of materials and methodology. Historically, this has been the rule when a novel technology is introduced in the field of biology; a valid example has been the 2D cell and tissue culture that started a century ago. Therefore, minimum standards must be established and adopted by the interested research community in order to advance the use of 3D culture.

After discussing the subject within the confines of our laboratory, we have concluded that funding agencies should provide a forum where the above referred standardization could be discussed, instigated and regulated using a consensus approach. We are aware that regulating research activities "from above" is risky, especially when not enough experience has been accumulated in the field to be regulated. However, we

believe that the past two decades of research with 3D cultures has generated sufficient knowledge and expertise in this area. Benign, tolerant and generally acceptable regulatory guidelines would prevent a chaotic situation where results from any of the many variables subject to change may be interpreted or misinterpreted as having to do with meaningful behavioral properties of the tissue being "created" or "reconstructed."

Now that biology at large is entering the post-genomic era while embracing a more organicist perspective, 3D cultures will undoubtedly become more relevant in our learning process. Standardization of the methodology in this field will facilitate the collection of data and their interpretation for the benefit of both science and technology.

APPENDIX I

Characterization of VA10 ALI Cultures

The immortalized bronchial epithelial cell line, VA10, was a generous gift of Dr. Thorarinn Gudjonsson [76]. VA10 cells were maintained in BEGM according to the authors' recommendations. Semi-confluent plates of VA10 cells were harvested with the addition of 3 ml of a 0.1 trypsin/1mM EDTA solution in PBS. Once the cells became freed from the culture vessel surface, the trypsin was inactivated by adding a sterile 2X solution of soybean trypsin inhibitor (STI) (Sigma), which was prepared by dissolving 500 mg STI into 500 ml F12 medium (Invitrogen).

1.5×10^5 viable VA10 cells were seeded onto the surface of type-IV collagen coated Millicell® PICM01250 cell culture inserts in a minimal volume of F12 medium (approximately 200 – 300 µl/insert). ALI medium was added to the culture plates containing the inserts, and placed in a humidified, 37°C incubator with 5% CO_2. The following day, 300 µl PBS was added to the surface of each insert and aspirated in order to remove non-adherent cells and cellular debris. ALI medium was replaced every second day, and liquid on the surface of the inserts was gently aspirated in order to maintain an air-liquid interface.

The cell-seeded inserts were cultured at an ALI for 2 weeks in order to promote functional differentiation of the epithelium. As a positive control for epithelial cell differentiation, 1.5×10^5 HBECs were seeded on Millicell® cell culture inserts that were pre-coated with 5 µg type-IV collagen. All experiments were performed in triplicate.

The inserts were harvested following 2 weeks of culture at an ALI. The inserts were placed in 10% formalin in PBS, processed with an automatic tissue processor containing a xylene alternative (SlideBright™; American Bio-Safety), and embedded in paraffin for subsequent immunohistochemical analyses. All antigen–antibody reactions were visualized using the streptavidin–peroxidase complex with diaminobenzidine tetrahydrochloride (DAB) (Sigma). Tissues were counterstained with Mayer's hematoxylin. Tissues were visualized and images were captured with a Zeiss Axioscope 2 Plus microscope fitted with an AxioCam HRc color CCD camera (Carl Zeiss).

VA10 cells formed a stratified epithelium that stained positively for cytokeratins (PanK) (Fig 11A). The columnar epithelium marker keratin 18 (K18) appeared scattered throughout the tissue and was not limited to the apical region (Fig 11B). Likewise, the basal epithelial cell marker, P63, was scattered throughout the tissue and was not limited to the basal region (Fig 11C). The cell-cell adhesion protein, E-cadherin (E-cad), was expressed normally throughout the tissue (Fig 11D).

Our results dispute the claim that the immortalized cell line, VA10, forms a pseudostratified epithelium when cultured at an air-liquid interface. Instead, we demonstrated that the epithelium is cuboidal and stratified, and that the typical bronchial epithelial cell markers are misexpressed throughout the tissue. Due to these results, along with an absense of ciliated and secretory epithelial cells (personal observation), we believe that VA10 is not a suitable cell line for 3D studies requiring a properly differentiated bronchial epithelium.

Fig 11

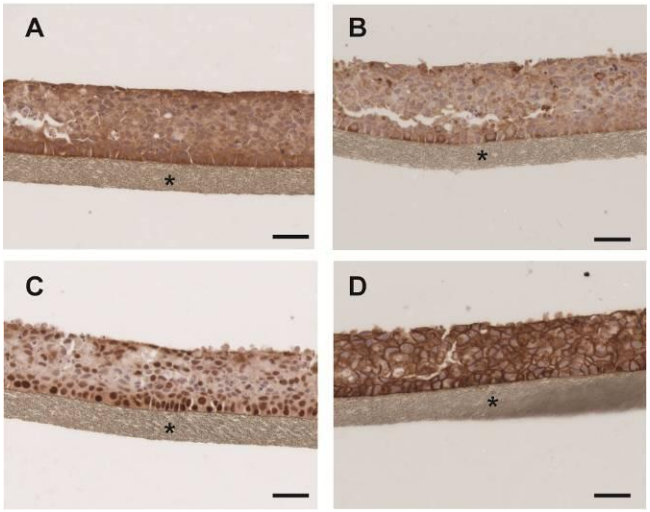

Figure 11. Characterization of VA10 cells cultured at an ALI on type-IV collagen coated inserts. Positive immunostaining for cytokeratins (PanK) indicated that VA10 cells are epithelial (11A). Keratin 18 (K18) immunostaining was scattered throughout the tissue and not limited to the apical region (11B). P63 immunostaining was also scattered and not limited entirely to the basal region (11C). Cells stained positively for E-cadherin (E-cad) along cell-cell junctions (11D). Morphologically, VA10 generated stratified cuboidal epithelia.

APPENDIX II

A549 is Contaminated with Alveolar Macrophages

A549 is a tumorigenic human cell lined derived in 1972 from an explanted pulmonary alveolar adenocarcinoma [123]. A549 are cuboidal in morphology, contain lamellar bodies and secrete surfactant proteins, as determined by phase contrast, electron microscopy and the incorporation of radio-labeled metabolic precursors, respectively [124]. Based on these studies and others [125, 126], A549 was found to be a suitable *in vitro* model cell line for studies of type II alveolar epithelial cell biology and surfactant biosynthesis and secretion.

More recent studies reported that A549 expresses low levels of the colony-stimulating factor receptor (CSF-1R) and that exogenously added colony stimulating factor (CSF-1) increases the invasiveness of this cell line [127, 128]. Also known as macrophage-colony stimulating factor (M-CSF), CSF-1 is the principal regulator of macrophage proliferation, differentiation and survival [129-132]. Macrophages are phagocytic leukocytes which differentiate from monocytes [133]. Their primary role is to engulf microbes and cellular debris and to communicate with and activate other immune cells through antigen presentation and the secretion of cytokines. Macrophages can be identified by the expression of cell surface makers, such as CD14, MAC-1 and CD68.

Macrophages can be found in most tissues of the body, including the lung, with the greatest pulmonary concentration existing in the alveoli of smokers [134]. In response to injury, alveolar epithelial cells attract monocytes and macrophages via the secretion of chemokines, such as GMCSF, RANTES, and MCP-1 (CCL2) [135]. In addition to

participating in immune surveillance and recovery from infection and injury, macrophages may exacerbate chronic conditions, such inflammation and cancer [136-138].

We report that the human continuous cell line, A549, is contaminated by alveolar macrophages. Alveolar macrophages were identified ultrastructurally by scanning electron microscopy, which was confirmed and quantified by flow-activated cell sorting (FACS) using an anti-CD68 antibody (Figure 12). Alveolar macrophages constituted 0.64% of the total cell population, which was significantly greater than the negative control sample that was incubated and sorted with an IgG control antibody (Chi-square test, $P < 0.0001$, $N = 3$). The presence of macrophage contamination in A549 suggests that previous reports describing A549 as having macrophage-like characteristics may require reinterpretation. In addition, many additional observations and results may need to be reconsidered as having been either directly or indirectly mediated by macrophages rather than A549 cells.

This report invokes additional questions, such as for how long has A549 been contaminated with macrophages? Presumably, from its inception, but how has this minor population of cells been maintained along with A549 for nearly 40 years? Did we observe an immortalized macrophage cell line, or did we observe macrophages that differentiated from an immortalized monocyte that has harmoniously co-existed with A549 since it was first derived in 1972. We hope that future experiments will clarify these queries.

Fig 12

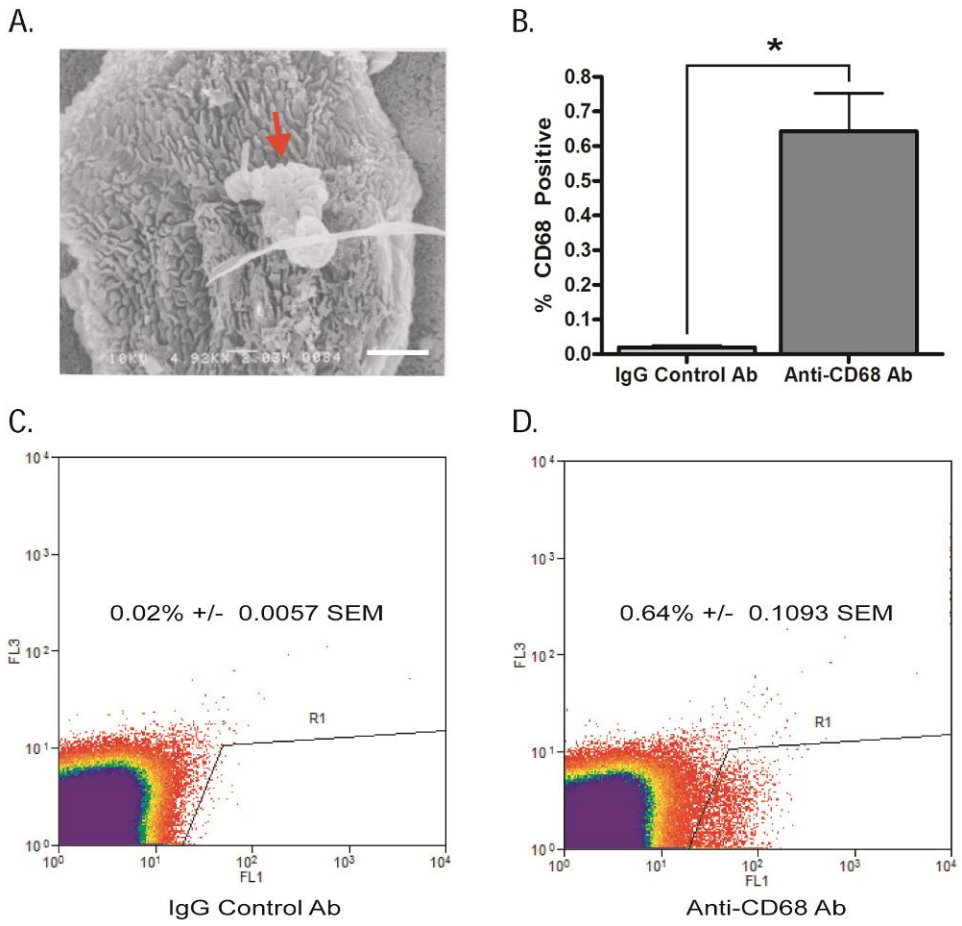

Figure 12.The cell line A549 is contaminated with alveolar macrophages. A Scanning electron micrograph of an alveolar macrophage present in A549 3D cultures (12A). Bacteria appear sequestered on the surface of the macrophage (red arrow). Flow activated cell sorting (FACS) analysis using a fluorescently-labeled anti-CD68 antibody confirms the presence of alveolar macrophages (12D) compared to samples sorted with an labeled IgG control antibody (12C). Analysis of the FACS data confirms that there are significantly more CD-68 positive sorting events in CD-68 labeled samples than in the IgG labeled control samples (Figure 12B, Chi-square test, $P < 0.0001$, $N = 3$).

APPENDIX III

Establishment and Characterization of the Cell Line HREC1.1

Lung cancer is the most common cause of cancer-related mortality world-wide [94, 139]. This can be explained, in part, by the fact that most individuals are diagnosed with an advanced disease, at which point clinical intervention is unlikely to provide a cure [140]. The most common type of lung cancer is non-small cell lung cancer (NSCLC), which can be further subdivided into squamous cell carcinoma, large cell carcinoma, and adenocarcinoma [26]. When treatment is an option, the heterogeneous nature of lung cancers makes choosing the appropriate type of therapy and/or surgery crucial [141]. Confounding these choices are the fact that NSLCs are known to express estrogen receptors and proliferate in response to E2 [142-144].

In this study, we describe a new human epithelial cell line (HREC-1.1) derived from explanted normal lung tissue obtained from lung cancer resection surgery. In two-dimensional (2D) cell culture, these cells appear polygonal in shape and form a stratified squamous epithelium when cultured at an air-liquid interface (ALI) on three-dimensional (3D) type-I collagen gels. Immunohistochemical analysis confirmed the presence of a basement membrane and the expression of epithelial makers. The cell line was sub-cloned, and cytogenetic analysis revealed that the parental HREC1.1 cell line had a modal chromosomal number of 69, and one of its sub-clones (E12) displayed numerous double minute chromosomes. Growth kinetics of the parental cell line and its clones were determined, and the parental cell line has been maintained in culture for more than 60 passages with no observable changes in morphology and/or phenotype.

MATERIALS AND METHODS

Human lung biopsy

On 09/12/2007, a 1.5 x 2 x 4 cm piece of normal human peripheral lung was surgically removed from a 79 year-old female patient undergoing elective mediastinoscopy, bronchoscopy and right upper lobectomy to remove a 1 x 1 x 0.9 cm mass diagnosed as a tumor. The normal lung tissue was placed in sterile saline and immediately prepared for explant culture.

Primary cell culture techniques and media

The normal lung tissue was washed twice with sterile phosphate buffered saline (PBS) and transferred to a sterile 100 mm tissue culture dish (BD Biosciences; San Jose, CA, USA) in a biological safety cabinet. Using crossed scalpels, the tissue was minced into pieces measuring approximately 0.4 cm^3. The pieces were transferred to 35 mm tissue culture dishes that had been pre-coated with an aqueous collagen/fibronectin/bovine serum albumin (BSA) solution. This solution contained 6 µg/ml human placental (type IV) collagen (Sigma), 1 µg/ml bovine fibronectin (Sigma), and 10.0 µg/ml bovine serum albumin (BSA) (Sigma). A scalpel was passed through each explanted tissue 1-3 times to promote adhesion to the plastic substrate.

The explants were fed either keratinocyte-serum free medium (K-SFM) (Invitrogen) or Dulbecco's-Modified Eagle Medium/F12 (D-MEM/F12) supplemented with 5% fetal bovine serum (FBS) (Hyclone) with media changes every other day, to select for epithelial cells and fibroblasts, respectively. Explants were kept in a humidified, 37°C incubator with 5% carbon dioxide (CO_2). If cells were observed

growing out from an explant, the tissue was removed once the cells reached a distance of approximately 1 cm from the tissue border. The cells were allowed to continue proliferating until they were approximately 90% confluent, at which point they were passaged at a ratio of 3:1 and given the designation passage 1 (P1). Excess passage 0 (P0) cells were re-suspended in DMEM/F12/5% FBS/10% dimethyl sulfoxide (DMSO) and frozen in liquid nitrogen. HREC1.1 was sub-cloned by limiting dilution.

Cell growth kinetics

On culture day 0, HBEC1.1 cells were seeded at a density of 1 x 10^4 cells/well in a 24-well tissue culture plate (BD Biosciences) and cultured for a total of 7 days with DMEM/F12/5% FBS replacement occurring every other day. Beginning on day 1, duplicate wells were harvested daily with 0.300 ml 0.5% trypsin-EDTA (Invitrogen). Trypsinization was stopped with the addition of 700 µl complete D-MEM/F12, and 200 µl aliquots were removed and transferred to particle cuvettes for cell counting. Cells were lysed with 2 ml 1X lysing solution (35.7 g ethylhexadecyldimethylammonium bromide, 1.23 g sodium chloride, 21 ml acetic acid, 750 ml Isoton II (Beckman Coulter; Fullerton, CA, USA), 10% (v/v) Triton X-100, 3.79 ml 4M magnesium chloride). Following lysis, 18-ml Isoton II was added to each cuvette, and the samples were counted with a Z2 particle counter (Becton Coulter). To determine whether HREC1.1 or its sub-clones proliferated in response to estrogen (E2), an E-screen assay was performed as described previously [145].

Cytogenetic analysis

HREC1.1 and its sub-clones (all passage 10) were seeded at a density of 0.75 x 10^6 cells/T25 flask. Two days later, 30 µl colcemid (10 µg/ml) (Invitrogen) was added to each flask and incubated for 20 minutes at 37^{o}C. After 20 minutes, the colcemid-containing medium was removed, and the cells were detached with trypsin, transferred to 15 ml conical tubes, and then centrifuged at 1100 RPM for 5 min. The supernatant was aspirated from the cell pellets, and 3 ml of a pre-warmed hypertonic solution (1:1 ratio of 0.075M potassium chloride and 0.6% sodium citrate) was added to each pellet. The pellets were gently re-suspended in the hypotonic solution and incubated for 20 minutes at room temperature (RT). After 20 minutes, 3 ml of ice-cold fixative (3:1 ratio of methanol and glacial acetic acid) was added and mixed by inverting the tubes three times. Metaphase chromosome spreads were prepared on glass slides from the fixed, pelleted cells. The spreads were baked and banded with trypsin and Wright-Giemsa. Twenty-one cells were counted from the parental cell line, HREC1.1, and karyotypes were prepared on twelve of the metaphases. For the three sub-clones, twenty cells were counted and karyotypes were prepared on five metaphases each. The karyotypes were described using ISCN 2005 nomenclature. Clonal changes seen in three or more metaphases were included, though not all cells had all changes. Fluorescence in situ hybridization (FISH) was performed on cells from E12, using a probe for MYC on chromosome 8 (Abbott Molecular; Downers Grove, IL, USA).

3D culture techniques

Bovine type I collagen (Organogenesis; Canton, MA, USA) was used at a final concentration of 1 mg/ml, and was neutralized and buffered with 1N sodium hydroxide

and 10X PBS according to the manufacturer's instructions. 3 ml of the collagen solution was dispensed into Transwell™ 24-mm inserts (Cat. No. 3414; Corning; Lowell, MA, USA) (3 ml/insert) placed within Deep-Well 6-well plates (BD Biosciences; San Jose, CA, USA) and allowed to polymerize at 37°C. Following polymerization, 1 x 10^6 HREC1.1 in 1 ml complete medium were seeded onto the surface of each collagen gel and 10 ml complete medium was placed in the wells below the insert. The plates were placed in a humidified, 37°C incubator with 5% CO_2. The culture medium was aspirated from the apical surface of the collagen gels on day 5 post-seeding, and the HREC1.1 were cultured at an air-liquid interface for an additional 2 weeks.

Histology and immunohistochemistry

On the day of harvest, the gels were removed from the Transwell™ inserts with a scalpel and cut into wedge-shaped sections. One piece was placed in 10% phosphate-buffered formalin, processed, and embedded in paraffin for subsequent analysis by histology and immunohistochemistry. A second piece was placed overnight in 2M sucrose, embedded in OCT mounting medium, and flash-frozen in liquid nitrogen for future analysis by immunohistochemistry. Histology stains included hematoxylin and eosin (H&E), periodic acid Schiff (PAS), and Masson's trichrome. Primary antibodies, suppliers, and working dilutions are listed in Table 4. Antibodies requiring antigen-retrieval are denoted with an asterisk. The antigen retrieval technique consisted of a microwave pretreatment in 0.01 M sodium citrate buffer (pH 6). All antigen–antibody reactions were visualized using the streptavidin–peroxidase complex with diaminobenzidine tetrahydrochloride (DAB) (Sigma). Tissues were counterstained with

Myer's hematoxylin. Images were captured using a Zeiss Axioscope 2 Plus microscope fitted with an AxioCam HRc color CCD camera (Carl Zeiss; Thornwood, NY, USA).

Scanning electron microscopy

The third and fourth gel wedges were fixed overnight in a neutral aqueous buffer containing 2.5% glutaraldehyde and 0.1 M sodium cacodylate. The fixed gels were post-fixed in 1% osmium tetroxide followed by dehydration to 100% ethanol. The samples were critical point dried under CO_2, mounted, and sputter-coated for viewing in a scanning electron microscope.

RESULTS

Patient medical history and clinical presentations

The patient was a 79 year-old female with a two-year history of increasing shortness of breath, which had worsened over a six month period. She had a medical history of hypertension, hypercholesterolemia, coronary artery disease, hypothyroidism, arthritis, osteoporosis, lumbar stenosis, and breast cancer. She had a family history of lung cancer, with her son dying from the disease. She had been a two-pack per day smoker for 40 years, but was no longer actively smoking. A chest CT scan showed no mediastinal lymphadenopathy, but identified a 1.2-cm nodule in the right upper lobe of her lung. A positron transmission tomography (PET) scan showed that the nodule was mildly active.

On 09/12/2007, she underwent elective mediastinoscopy, bronchoscopy and a right upper lobectomy to remove the mass. The 1 x 1 x 0.9 cm, 150 gram primary tumor

was surrounded by normal lung tissue, and had not invaded the visceral pleura. The tumor was sent for pathologic analysis, while a 1.5 x 2 x 4 cm piece of normal lung was placed in saline and immediately prepared for explant culture.

Pathologic analysis

The margins of excision were negative for invasion, but invasion was observed in some pulmonary artery branches in the region of the tumor. The primary tumor was found to be a poorly differentiated (Grade III) squamous cell carcinoma with a necrotic center. No specific staining for mucin was seen in the tumor cells by mucicarmine stain. Immunohistochemical stains for CK7, CD31, CAM 5.2, p63, CK5/6, TTF1, CK20 and CK34 beta E12 were performed to evaluate the specimen. The vast majority of tumor cells were positive for CAM 5.2, p63, CK5/6, CK34, beta E12, while most of the cells were negative for CK7. A few scattered cells were positive for CK20 while most of the tumor cells did not stain for CK20. The tumor cells showed no significant staining for TTF-1 or CD31. Overall, these features supported the diagnosis of a poorly differentiated squamous cell carcinoma (summarized in Table 5). The differential diagnosis would include a primary lung tumor even though the tumor cells are negative for TTF-1.

Cell growth kinetics

HREC1.1 and its clones displayed a similar pattern of cell growth, with a four day period of logarithmic growth and a population doubling time of approximately 16.4 hours (Figure 13A). HREC1.1 and its clones did not proliferate in the presence of E2 (Figure 13B).

Table 5. Pathologic analysis of the primary tumor	
Antibody	Positive (+)/Negative (-)
CK7	-
CD31	-
CAM 5.2	+
p63	+
CK5/6	+
TTF1	-
CK20	-
CK34 beta E12	+

Fig 13

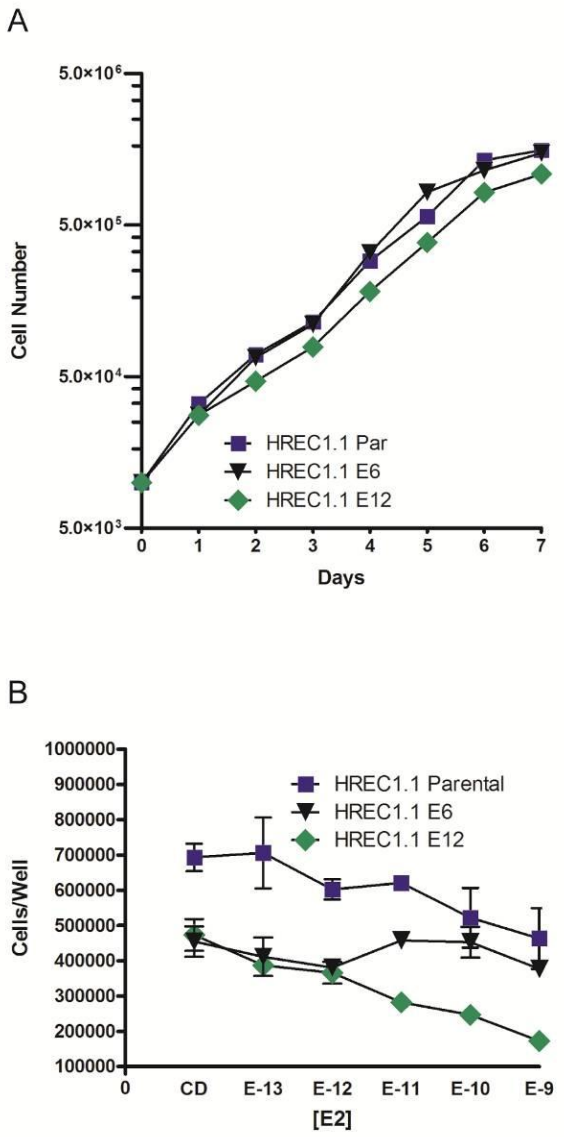

Figure 13. Growth kinetics of HREC1.1 and its clones. Parental HREC1.1 and clones E6 and E12 achieve similar maximal population densities when cultured for one week in growth medium (13A). These cells do not proliferate in response to estradiol (E2) (13B).

Cytogenetic analysis

The parental cell line, HREC1.1, was found to have a modal chromosome number of 69, range 63 – 73 chromosomes (Figure 14A). The karyotype was complex with multiple rearrangements (Figure 14B and Table 6). The three sub-clones were found to share many of the rearrangements seen in the parent cell line, but each sub-clone had at least one additional unique rearrangement. F4 had six unique additional rearrangements, E6 had one unique additional rearrangement and E12 had five unique additional rearrangements, summarized in Table 7. Sub-clone E12 was noted to have numerous double minutes (Figure 15), and a review of all cells identified a low level of double minutes in all lines. Fluorescence in situ hybridization (FISH) was performed on cells from E12, using a probe for MYC on chromosome 8 (MYC Abbott Molecular, Downers Grove, IL). The double minutes were negative for MYC (data not shown).

Fig 14

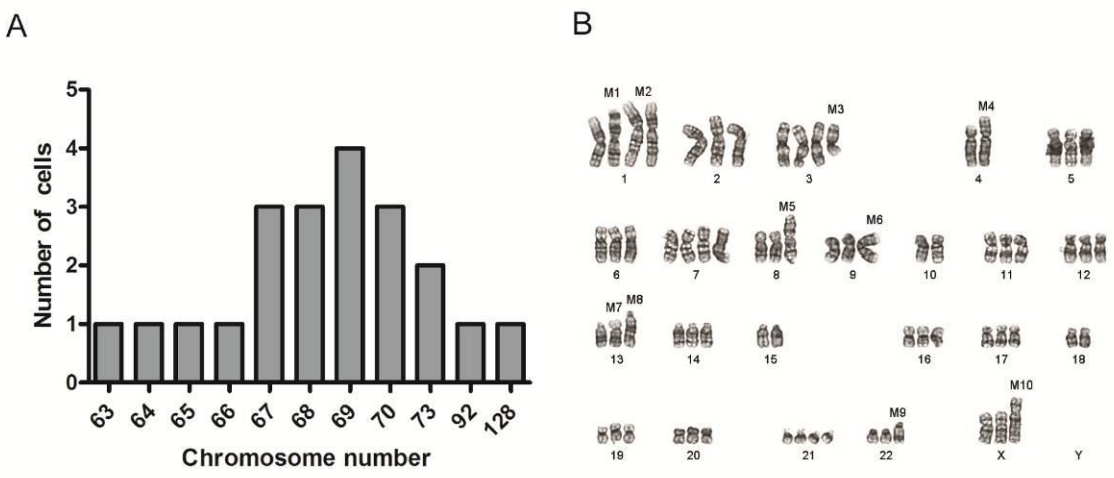

Figure 14. Cytogenetic analysis of HREC1.1 revealed multiple chromosomal rearrangements (14B) and a modal chromosome number of 69, with a range from 63 – 73 (14A).

Table 6. Karyotype of HREC1.1 and three sub-clones	
Cell Line	Karyotype
HREC1.1	67-73<3n>,XX,dup(X)(q22q26),der(1)t(1;15)(q42;q15)x2, +der(1)t(1;17)(p34;q21), der(3)t(1;3)(p34;q21), +der(3)t(3;6)(p21;p21.1), add(4)(q33),der(4)t(4;10)(p12;q11.2), der(8)t(X;8)(q13;p11.2),-9,psu dic(9)(p11.2),-10,+13,der(13)t(13;19)(q10;p10), dup(13)(q14q32),der(14)t(9;14)(q22;q32)-15,-18, +21,der(22)t(17;22)(q21;q13),+mar,0~2dmin[cp12]
HREC1.1 F4, passage 10	54-64<3n>,X,-X,dup(X)(q22q26),add(1)(q32), der(1)t(1;15)(q42;q15)x2,+der(1)t(1;17)(p34;q21), der(3)t(3;6)(p21;p21.1),der(3)t(3;14)(p25;q32),add(4)(q33),der(4)t(4;10)(p12;q11.2), der(7)t(7;15)(q31.2;q15), der(8)t(X;8)(q13;p11.2), -9,-10, del(11)(q13), der(13)t(13;19)(q10;p10)t(13;19)(q12;p13.3), dup(13)(q14q32),der(14)t(9;14)(q22;q32),-15,-17,-18,-19,-21.-22,0~30dmin[cp5]
HREC1.1 E6, passage 10	62-69<3n>,XX,dup(X)(q22q26), der(1)t(1;15)(q42;q15)x2,+der(1)t(1;17) (p34;q21), der(3)t(3;6)(p21;p21.1), add(4)(q33)der(4)t(4;10)(p12;q11.2), der(8)t(X;8)(q13;p11.2),-9,psu dic(9)(p11.2),-10, der(13)t(13;19)(q10;p10), dup(13)(q14q32),-15,-18,+19, der(20)t(15;20)(q13;q13.1), der(22)t(17;22)(q21;q13),+mar,3~10dmin[cp5]
HREC1.1 E12, passage 10	63-68<3n>,XX, dup(X)(q22q26), der(1)t(1;15)(q42;q15)x2,der(1)t(1;17)(p34;q21), der(3)t(1;3)(p34;q21),+der(3)t(3;6)(p21;p21.1), add(4)(q33),der(4)t(4;10)(p12;q11.2),der(8)t(X;8) (q13;p11.2),-9,psu dic(9)(p11.2),-10, der(13)t(13;19)(q10;p10),dup(13)(q14q32), der(14)t(7;14)(q21.2;q22),add(17)(p13), der(17)t(2;17)(q31;p13)dup(2)(q31q37),-18,-19, add(20)(p13),+21,11~49dmin[cp5]

Table 7. Summary of comparison of the three sub-clones and the parental line			
Description	F4	E6	E12
dup(X)(q22q26)	X	X	X
der(1)t(1;17)(p34;q21)	X	X	X
der(1)t(1;15)(q42;q15)	X	X	X
add(1)(q32)	X	-	-
der(3)t(1;3)(p34;q21)	-	-	X
der(3)t(3;6)(p21;p21.1)	X	X	X
der(3)t(3;14)(p25;q32)	X	-	-
der(4)t(4;10)(p12;q11.2)	X	X	X
add(4)(q33)	X	X	X
der(7)t(7;15)(q31.2;q15)	X	-	-
der(8)t(X;8)(q13;p11.2)	X	X	X
psu dic(9)(p11.2)	-	X	X
del(11)(q13)	X	-	-
der(13)t(13;19)(q10;p10)	-	X	X
der(13)t(13;19)(q10;p10)t(13;19)(q12;p13.3)	X	-	-
dup(13)(q14q32)	X	X	X
der(14)t(7;14)(q21.2;q22)	-	-	X
der(14)t(9;14)(q22;q32)	X	-	-
add(17)(p13)	-	-	X
der(17)t(2;17)(q31;p13)dup(2)(q31q37)	-	-	X
add(20)(p13)	-	-	X
der(20)t(15;20)(q13;q13.1)	-	X	-
der(22)t(17;22)(q21;q13)	-	X	X
Isochromosome of 8q with ?centromere	X	X	-
Marker	X	-	-

Fig 15

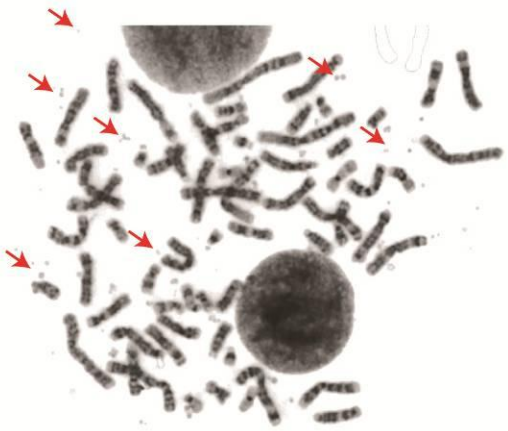

Figure 15. Chromosomal analysis revealed the presence of numerous double minute chromosomes (red arrows) in the HREC1.1 subclone E12.

Histology and immunohistochemistry

When cultured in 2D on tissue culture plastic, HREC1.1 was observed to have an epithelial morphology consisting of polygonal shaped cells with numerous filopodia (Figure 16A). When cultured at an ALI on 3D collagen gels, HREC1.1 formed a stratified squamous epithelium (Figure 16B – 16C). Supra-basal cells frequently stained positive for PAS (Figure 16C). Trichrome staining revealed areas of collagen production throughout the epithelium (Figure 16E – 16F). Immunohistochemical analysis demonstrated that some cells displayed positive staining for epithelial keratins (Pan-K) (Figure 16H, red arrows), and positive staining for keratin 18 was evident in both the apical and basal portion of the epithelium (Figure 16I, red arrows). Positive staining for the epithelial marker p63 was observed in the cytoplasm of some cells (Figure 16J). The tissue did not stain positive for keratins 10 (CK10), 13 (CK13), or keratins 1, 5, 10 and 14 (CK34 beta E12) (Figure 16K – 16M). Cells did not express the cell-cell adhesion protein E-cadherin (E-cad) or the endothelial cell marker CD31 (Figure 16N – 16O). A

basement membrane was apparent beneath the basal portion of the tissue, as evidenced by positive type-IV collagen (Col IV) staining (Figure 16P). See Table 8 for primary antibodies and working dilutions.

Fig 16

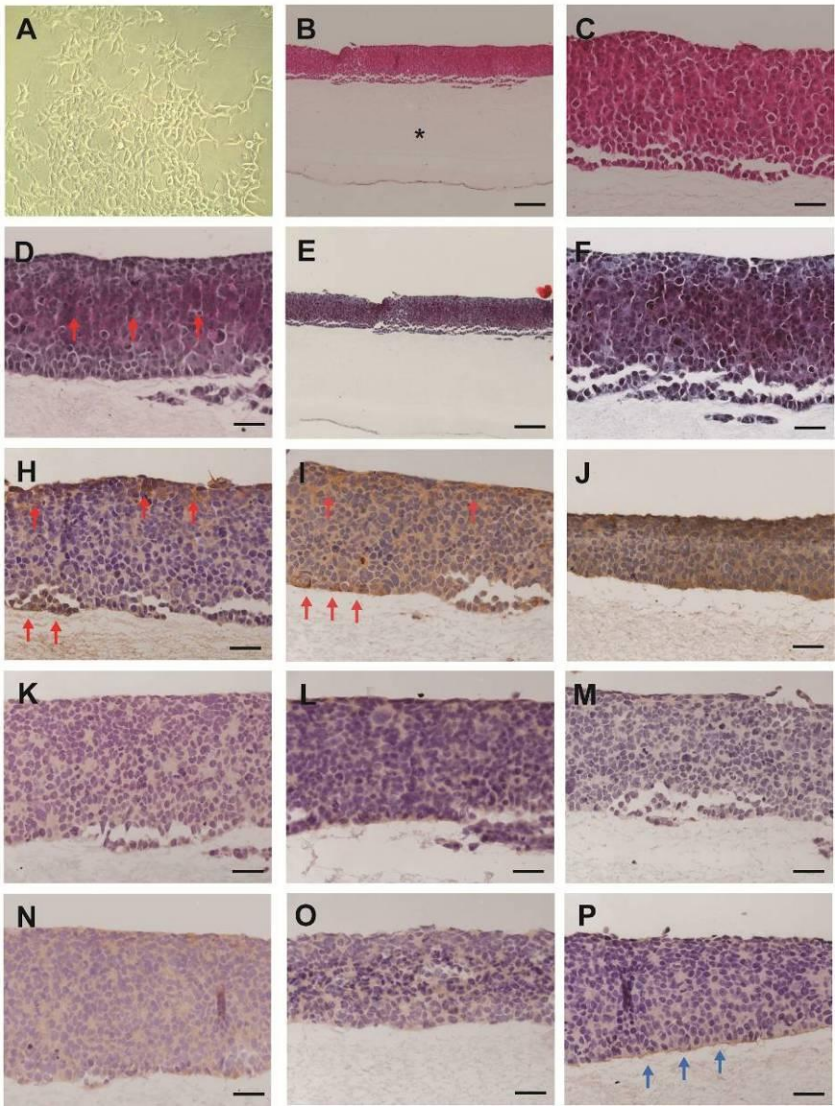

Figure 16. Microscopic, histological, and immunohistochemical analysis of HREC1.1. HREC1.1 has a polygonal epithelial morphology when cultured in 2D (16A), but forms a stratified cuboidal epithelium when cultured on 3D collagen gels, as evidenced by staining with hematoxylin and eosin (H&E) (16 A – 16B). Areas of carbohydrate synthesis were evident following staining with periodic acid Schiff's (PAS) reagent (red arrows, 16D), and Trichrome staining demonstrates areas of collagen accumulation (16E – 16F). Immunohistochemical analysis confirmed that the cells express cytokeratins (PanK) (red arrows, 16H), with some cells expressing keratin 18 (K18) (red arrows, 16I). Cytoplasmic P63 staining was observed in some cells (16J). The cells did not stain positively for keratins 10 (16K), 13 (16L), or 1, 5, 10, and 14 (CK34 beta E12) (16M). Likewise, the cells did not express E-cadherin (E-cad) (16N), CD31 (16O), but stained positive for type-IV collagen (blue arrows, 16P). Scale bars = 160 µm (16B and 16F) and 40 µm (16C, 16D, and (16F – 16P).

Ultrastructural analysis

High resolution scanning electron micrographs demonstrated that HREC1.1 cells generate stratified tissues in 3D ALI cultures (Figure 5A – 5B), and that the morphology of HREC1.1 varies from cuboidal (5B, red arrow) to squamous (5B, yellow arrow).

Table 8. Primary antibodies, suppliers, and working dilution

Antigen*	Supplier	Cat. No./Clone	Specie	Dilution
CK10*	Abcam	AB20121	Mouse	1:200
CK13*	Abcam	AB22685	Mouse	1:400
CK1/5/10/14*	Novovastra	NCL-CK34BE12	Mouse	1:100
CK18*	Sigma	C8541	Mouse	1:100
P63*	Santa Cruz	SC-8431	Mouse	1:100
E-cadherin*	Novocastra	NCL-E-Cad	Mouse	1:75
Type IV collagen*	DakoCytomation	AF5610	Mouse	1:50
CD31	Abcam	AB54211	Mouse	1:500

Fig 17

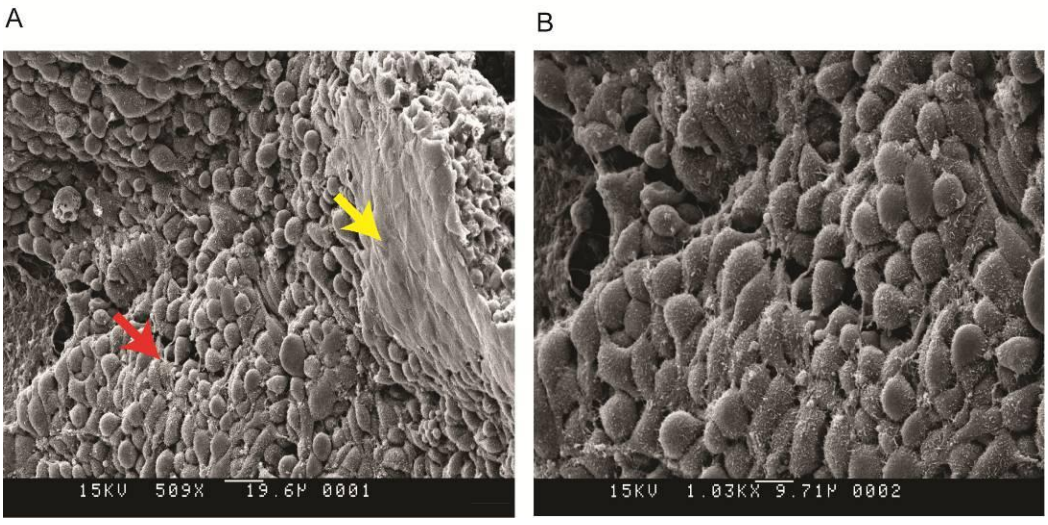

Figure 17. Ultrastructural analysis of HREC1.1 cultured on 1 mg/ml bovine type-I collagen gels. HREC1.1 appeared cuboidal (red arrow) with flat, squamous regions present at the apical surface of the epithelium. Scale bars represent 19.6 µm (A) and 9.71 (B).

APPENDIX IV

Analysis of Type-I Collagen Enzymatic Cross-Linkers

We explored enzymatic collagen cross-linkers as a potential means of stabilizing the type-I collagen matrices in order to prevent cell-mediated contraction of the collagen gels. The main advantage of using enzymatic cross-linkers over chemical cross-linkers is that they are considered non-cytotoxic, which allows them to be incorporated into the collagen matrices in the presence of cells. Two enzymes have been reported to cross-link various members of the collagen superfamily – tissue transglutaminase (TGase) and lysyl-oxidase (LOX) [113-115]. From these two options, transglutaminase was selected due to its availability and price.

Transglutaminase purified from guinea pig livers was purchased as a lyophilized powder and was reconstituted according to the manufacturer's instructions (Sigma-Aldrich Corp.; St. Louis, MO, USA). A buffered aqueous solution of rat tail type-I collagen (1 mg/ml) was prepared as described previously, and combined with the reconstituted transglutaminase in the following (w/w) ratios: 100:1; 500:1; 1000:1; 1:0. The collagen/transglutaminase solutions were dispensed into 24-well multi-well plates (0.5 ml/well) and allowed to polymerize in a 37ºC incubator. Following polymerization, the free-amine content was determined using the trinitrobenzenesulfonic acid (TNBS) assay [146].

The TNBS assay is based on the principle that TNBS reacts with primary amine groups in aqueous solutions and forms yellow adducts which can be quantified using a spectrophotometer. A solution of TNBS was added to each well and the plate was returned to the 37ºC incubator for an additional 2 hours. Following the two hour

incubation, the gels were solubilized with 6M HCL, dispensed into a 96-well plate, and the absorbance was measured at 340 nm with a spectrophotometer (Bio-Rad; Hercules, CA, USA). The addition of transglutaminase to the collagen solutions resulted in no decrease in the free amine content compared to non-cross-linked controls, indicating that transglutaminase is not a cross-linker of type-I collagen (Figure 18). This experiment has been repeated a total of three times with similar results.

At this time, transglutaminase does not appear to be a viable type-I collagen cross-linker, leaving lysyl oxidase as the only remaining enzymatic alternative. Unfortunately, lysyl oxidase is not commercially available as either a purified or recombinant protein, and therefore must be expressed from a cDNA clone and purified by the end user. These additional steps and costs make it prohibitively expensive for us to consider lysyl oxidase at present.

Fig 18

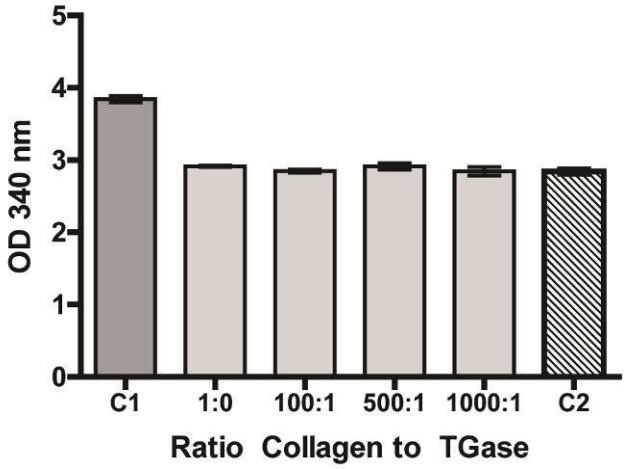

Figure 18. TNBS assay to determine free amine content of TGase treated collagen gels. Collagen was combined with reconstituted TGase in (w/w) ratios of 1:0, 100:1, 500:1, 1000:1. C1 = 1 mg/ml glycine control. C2 = 0.25 mg/ml glycine control.

APPENDIX V

Analysis of Alternatives to Collagen-Based Matrices

Alternatives to type-I collagen were explored as a means of creating a 3D culture environment that could not be contracted by HBECs or lung fibroblasts. In considering our options, we understood that our choices would be limited to only those in which collagen could be incorporated, because it has been demonstrated that type-I and/or type-IV collagen are necessary for HBEC adhesion. With this in mind, we selected synthetic peptide hydrogels and silk fibroin-based scaffolds to test.

PuraMatrix™ (BD Biosciences; San Jose, CA, USA) is a synthetic matrix consisting of 1% (w/v) amino acids and 99% water. In the presence of salts, it self-assembles into a hydrogel that has been used in the 3D culture of a variety of cell types, including both established cell lines and primary cells [147, 148]. To test whether PuraMatrix™ is a suitable matrix for the 3D culture of HBECs, HBECs were cultured on hydrogels consisting of either PuraMatrix™ alone, PuraMatrix™ + rat tail type-I collagen, or PuraMatrix™ + synthetic RGD peptides using methods similar to those described previously.

Briefly, lung fibroblasts (IMR-90 or LuCAF) were resuspended in 20% sucrose and combined 1:1 with 1% PuraMatrix™ to produce a 0.5% solution of PuraMatrix™ and cells. To these solutions, aqueous type-I collagen (1 mg/ml) or synthetic RGD peptides were added in a 1:6 ratio, according to the manufacturer's recommendations. To test whether PuraMatrix™ alone was sufficient for HBEC adherence, a solution of PuraMatrix™ without type-I collagen or RGD peptides was prepared. The PuraMatrix™ solutions were pipetted into Millicell® PICM01250 cell culture inserts (Millipore,

Billerica, MA) placed within the wells of 6-well culture plates (≤ 3 inserts/well) and allowed to polymerize in the presence of BEGM. Following polymerization, 150,000 HBECs were seeded on the surface of the gels. As a control, 150,000 HBECs were seeded into type-IV collagen coated Millicell® inserts.

The following day, the gels and inserts were observed with an inverted microscope to evaluate whether the HBECs adhered to their substrates. HBECs adhered to the coated cell culture inserts but did not adhere to the 0.5% PuraMatrix™ gels, as evidenced by the presence of considerable floating cells and cellular debris (Figure 2). HBECs appeared to adhere well to the 0.5% PuraMatrix™ + type-I collagen gels, but adhered less to the 0.5% PuraMatrix™, as evidenced by a mix or adherent cells and cellular debris (Figure 19). While these results were promising, adherent cells were present only on the coated cell culture inserts at 72 hours post-seeding. These results indicate that the conditions provided by the PuraMatrix™ peptide hydrogels were not sufficient for HBEC attachment and survival. Additional experiments could be performed with increased concentrations of type-I collagen and/or RGD peptides to identify suitable HBEC culture conditions.

Silk fibroin-based scaffolds have been used in three-dimensional cell culture and tissue engineering to generate tissues that morphologically and functionally resemble a variety of human tissues and organs [149-153]. In addition to silk's low immunogenicity and high biocompatibility, other qualities of silk that make it desirable for tissue engineering applications are that the scaffold porosity and degradation rates can be easily controlled. In addition, silk scaffolds can be coated with extracellular matrix proteins to enhance cell adhesion and survival.

To determine whether silk-based scaffolds are suitable for HBEC 3D culture, we selected silk fibroin sponges in which the silk fibroin had been solubilized with either an aqueous (water-based) or a 1,1,1,3,3,3-hexafluoro-2-propanol (HFIP) (HFIP-based) solution. The average pore diameter of the aqueous- or HFIP-based sponges ranged from 400 – 600 µm. Cylinders (9 mm diameter x 4 mm height) were cut from the silk sponges with a #5 cork borer, sterilized, and placed into Millicell® PICM01250 cell culture inserts. A solution of 1 mg/ml rat tail type-I collagen (with or without lung fibroblasts) was pipette into each well (300 µl/well) and allowed to polymerize overnight. The following day, 150,000 HBECs were seeded onto each silk/collagen scaffold and cultured for 2 weeks at an air-liquid interface (ALI). As a control, 150,000 HBECs were seeded into type-IV collagen coated Millicell® inserts.

When observed microscopically with an inverted microscope, beating cilia were present on the surface of type-IV collagen coated inserts but could not be seen on the surface of type silk/collagen cylinders. In addition, the persistence of culture medium on the surface of the cylinders suggested that a surface epithelium had not formed. When examined histologically, fibroblasts were seen in some areas of the silk/collagen scaffolds, but an epithelium was not evident on the surface (data not show). Taken together, these results suggest that despite the defined porosity and biomechanical properties of silk fibroin sponges, they are not an ideal matrix for the 3D culture of bronchial epithelial cells. A possible reason for this is that the nutrient transport is inhibited by the silk/collagen scaffold, and future studies could be designed to maximize transport by increasing porosity, decreasing the volume of the scaffolds, or incorporating a perfusion bioreactor.

Fig 19

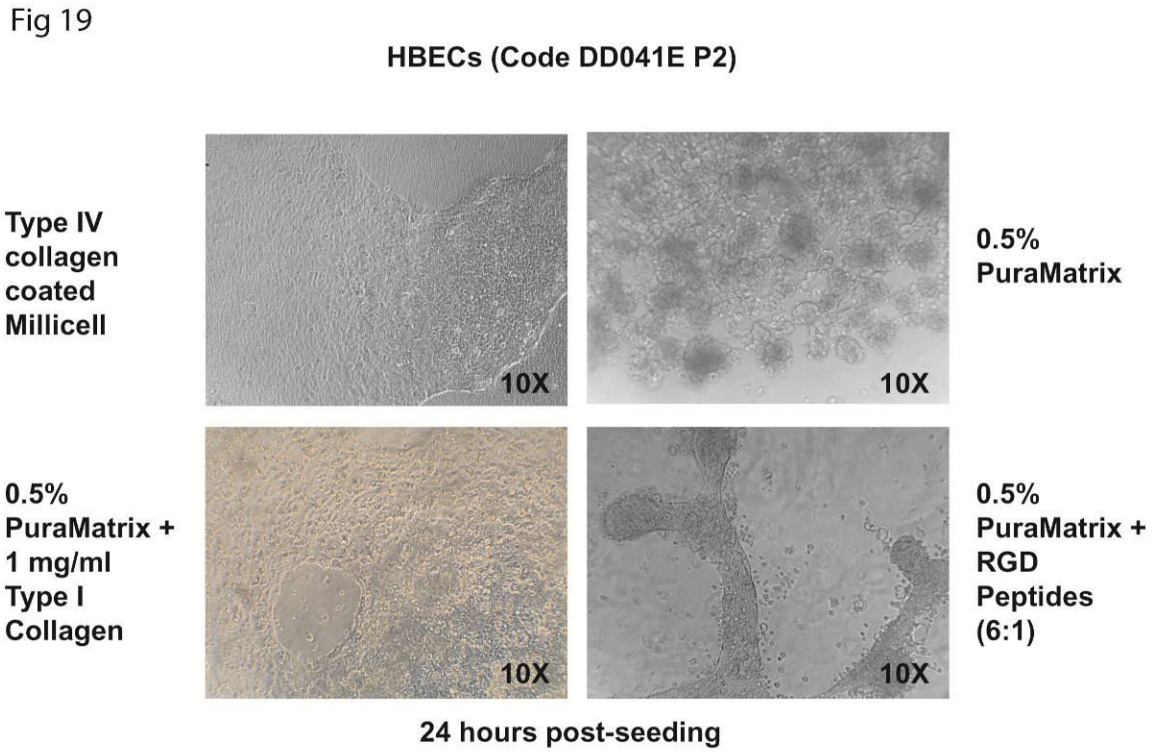

Figure 19. Analysis of PuraMatrix hydrogels as putative 3D matrices for HBEC culture. 150,000 HBECs (Code DD041E, P2) were cultured on the surface of hydrogels composed of 0.5% PuraMatrix, 0.5% PuraMatrix + 1 mg/ml type-I collagen, or 0.5% PuraMatrix + RGD peptides (6:1 molar ratio). The gels were examined with an inverted microscope 24 hours post-seeding. HBECs adhered well to 0.5% PuraMatrix + 1 mg/ml type-I collagen gels in a manner that was comparable to type-IV collagen coated Millicells, but did not adhere to either PuraMatrix alone or PuraMatrix + RGD peptides.

APPENDIX VI

Published Manuscripts

Pageau, S.C., et al., *The effect of stromal components on the modulation of the phenotype of human bronchial epithelial cells in 3D culture.* Biomaterials, 2011. 32(29): p. 7169-80.

BIBLIOGRAPHY

1. Ingber, D., *Integrins as mechanochemical transducers.* Curr Opin Cell Biol, 1991. **3**(5): p. 841-8.
2. Soto, A.M. and C. Sonnenschein, *The tissue organization field theory of cancer: a testable replacement for the somatic mutation theory.* Bioessays. **33**(5): p. 332-40.
3. Maffini, M.V., et al., *Stromal regulation of neoplastic development: age-dependent normalization of neoplastic mammary cells by mammary stroma.* Am J Pathol, 2005. **167**(5): p. 1405-10.
4. Maffini, M.V., et al., *The stroma as a crucial target in rat mammary gland carcinogenesis.* J Cell Sci, 2004. **117**(Pt 8): p. 1495-502.
5. Warburton, D. and M.K. Lee, *Current concepts on lung development.* Curr Opin Pediatr, 1999. **11**(3): p. 188-92.
6. Sanchez-Esteban, J., et al., *Effects of mechanical forces on lung-specific gene expression.* Am J Med Sci, 1998. **316**(3): p. 200-4.
7. Torday, J.S., J. Sanchez-Esteban, and L.P. Rubin, *Paracrine mediators of mechanotransduction in lung development.* Am J Med Sci, 1998. **316**(3): p. 205-8.
8. Rudnick, D., *Developmental capacities of the chick lung in chorioallantoic grafts.* J Exp Zool, 1933. **66**: p. 125-154.
9. Lawson, K.A., *The role of mesenchyme in the morphogenesis and functional differentiation of rat salivary epithelium.* J Embryol Exp Morphol, 1972. **27**(3): p. 497-513.
10. Lawson, K.A., *Mesenchyme specificity in rodent salivary gland development: the response of salivary epithelium to lung mesenchyme in vitro.* J Embryol Exp Morphol, 1974. **32**(2): p. 469-93.
11. Wessells, N.K., *Mammalian lung development: interactions in formation and morphogenesis of tracheal buds.* J Exp Zool, 1970. **175**(4): p. 455-66.
12. Sakakura, T., Y. Nishizuka, and C.J. Dawe, *Mesenchyme-dependent morphogenesis and epithelium-specific cytodifferentiation in mouse mammary gland.* Science, 1976. **194**(4272): p. 1439-41.
13. Shannon, J.M., *Induction of alveolar type II cell differentiation in fetal tracheal epithelium by grafted distal lung mesenchyme.* Dev Biol, 1994. **166**(2): p. 600-14.
14. Shannon, J.M., et al., *Mesenchyme specifies epithelial differentiation in reciprocal recombinants of embryonic lung and trachea.* Dev Dyn, 1998. **212**(4): p. 482-94.
15. Parent, R.A., *Treatise on pulmonary toxicology*. 1992, Boca Raton: CRC Press. v. <1 >.
16. Ross, M.H., E.J. Reith, and L.J. Romrell, *Histology : a text and atlas*. 2nd ed. 1989, Baltimore: Williams & Wilkins. xx, 783 p.
17. Evans, M.J., et al., *The role of basal cells in attachment of columnar cells to the basal lamina of the trachea.* Am J Respir Cell Mol Biol, 1989. **1**(6): p. 463-9.
18. Merker, H.J., *Morphology of the basement membrane.* Microsc Res Tech, 1994. **28**(2): p. 95-124.

19. Merker, H.J. and H.J. Barrach, *The morphology of basement membrane formation.* Eur J Cell Biol, 1981. **26**(1): p. 111-20.
20. Brewster, C.E., et al., *Myofibroblasts and subepithelial fibrosis in bronchial asthma.* Am J Respir Cell Mol Biol, 1990. **3**(5): p. 507-11.
21. Evans, M.J., et al., *Attenuated fibroblast sheath around the basement membrane zone in the trachea.* Am J Respir Cell Mol Biol, 1993. **8**(2): p. 188-92.
22. Clark, R.A.F., *The molecular and cellular biology of wound repair*. 2nd ed. The language of science. 1996, New York: Plenum Press. xxiii, 611 p., [1] leaf of plates.
23. Gizycki, M.J., et al., *Myofibroblast involvement in the allergen-induced late response in mild atopic asthma.* Am J Respir Cell Mol Biol, 1997. **16**(6): p. 664-73.
24. Zhang, S., P.H. Howarth, and W.R. Roche, *Cytokine production by cell cultures from bronchial subepithelial myofibroblasts.* J Pathol, 1996. **180**(1): p. 95-101.
25. Jemal, A., et al., *Cancer statistics, 2007.* CA Cancer J Clin, 2007. **57**(1): p. 43-66.
26. Ihde, D.C. and J.D. Minna, *Non-small cell lung cancer. Part I: Biology, diagnosis, and staging.* Curr Probl Cancer, 1991. **15**(2): p. 61-104.
27. Breuer, R.H., et al., *The natural course of preneoplastic lesions in bronchial epithelium.* Clin Cancer Res, 2005. **11**(2 Pt 1): p. 537-43.
28. Wistuba, II and A.F. Gazdar, *Lung cancer preneoplasia.* Annu Rev Pathol, 2006. **1**: p. 331-48.
29. Fontana, R.S., et al., *Lung cancer screening: the Mayo program.* J Occup Med, 1986. **28**(8): p. 746-50.
30. Marcus, P.M., et al., *Lung cancer mortality in the Mayo Lung Project: impact of extended follow-up.* J Natl Cancer Inst, 2000. **92**(16): p. 1308-16.
31. Manser, R.L., et al., *Incidental lung cancers identified at coronial autopsy: implications for overdiagnosis of lung cancer by screening.* Respir Med, 2005. **99**(4): p. 501-7.
32. Bach, P.B., *Is our natural-history model of lung cancer wrong?* Lancet Oncol, 2008. **9**(7): p. 693-7.
33. Hamilton, A.E., *This smoking world*. 1927, New York,: The Century Co. xvii, 227 p.
34. Doll, R. and A.B. Hill, *Smoking and carcinoma of the lung; preliminary report.* Br Med J, 1950. **2**(4682): p. 739-48.
35. United States. Surgeon General's Advisory Committee on Smoking and Health., *Smoking and health; report of the advisory committee to the Surgeon General of the Public Health Service*. 1964, [Washington]: U.S. Dept. of Health, Education, and Welfare, Public Health Service; [for sale by the Superintendent of Documents, U.S. Govt. Print. Off. xvii, 387 p.
36. Wald, N.J. and A.K. Hackshaw, *Cigarette smoking: an epidemiological overview.* Br Med Bull, 1996. **52**(1): p. 3-11.
37. Smith, C.J., S.D. Livingston, and D.J. Doolittle, *An international literature survey of "IARC Group I carcinogens" reported in mainstream cigarette smoke.* Food Chem Toxicol, 1997. **35**(10-11): p. 1107-30.
38. Hecht, S.S., *Tobacco smoke carcinogens and lung cancer.* J Natl Cancer Inst, 1999. **91**(14): p. 1194-210.

39. Culp, S.J., et al., *A comparison of the tumors induced by coal tar and benzo[a]pyrene in a 2-year bioassay.* Carcinogenesis, 1998. **19**(1): p. 117-24.
40. Hecht, S.S., *Biochemistry, biology, and carcinogenicity of tobacco-specific N-nitrosamines.* Chem Res Toxicol, 1998. **11**(6): p. 559-603.
41. Coggins, C.R., *A review of chronic inhalation studies with mainstream cigarette smoke in rats and mice.* Toxicol Pathol, 1998. **26**(3): p. 307-14; discussion 315.
42. Yuan, H., E.P. Ingenito, and B. Suki, *Dynamic properties of lung parenchyma: mechanical contributions of fiber network and interstitial cells.* J Appl Physiol, 1997. **83**(5): p. 1420-31; discussion 1418-9.
43. Choe, M.M., P.H. Sporn, and M.A. Swartz, *An in vitro airway wall model of remodeling.* Am J Physiol Lung Cell Mol Physiol, 2003. **285**(2): p. L427-33.
44. Choe, M.M., P.H. Sporn, and M.A. Swartz, *Extracellular matrix remodeling by dynamic strain in a three-dimensional tissue-engineered human airway wall model.* Am J Respir Cell Mol Biol, 2006. **35**(3): p. 306-13.
45. Wirtz, H.R. and L.G. Dobbs, *Calcium mobilization and exocytosis after one mechanical stretch of lung epithelial cells.* Science, 1990. **250**(4985): p. 1266-9.
46. Winters, S.L., C.W. Davis, and R.C. Boucher, *Mechanosensitivity of mouse tracheal ciliary beat frequency: roles for Ca2+, purinergic signaling, tonicity, and viscosity.* Am J Physiol Lung Cell Mol Physiol, 2007. **292**(3): p. L614-24.
47. Grainge, C.L., et al., *Effect of bronchoconstriction on airway remodeling in asthma.* N Engl J Med. **364**(21): p. 2006-15.
48. Horowitz, J.C. and V.J. Thannickal, *Epithelial-mesenchymal interactions in pulmonary fibrosis.* Semin Respir Crit Care Med, 2006. **27**(6): p. 600-12.
49. Ebihara, T., et al., *Changes in extracellular matrix and tissue viscoelasticity in bleomycin-induced lung fibrosis. Temporal aspects.* Am J Respir Crit Care Med, 2000. **162**(4 Pt 1): p. 1569-76.
50. Brody, A.R., et al., *Epithelial-mesenchymal associations of cells in human pulmonary fibrosis and in BHT-oxygen-induced fibrosis in mice.* Exp Lung Res, 1981. **2**(3): p. 207-20.
51. Pageau, S.C., et al., *The effect of stromal components on the modulation of the phenotype of human bronchial epithelial cells in 3D culture.* Biomaterials.
52. Castello-Cros, R., et al., *Matrix remodeling stimulates stromal autophagy, "fueling" cancer cell mitochondrial metabolism and metastasis.* Cell Cycle. **10**(12): p. 2021-34.
53. Hoshino, A., et al., *Podoplanin-positive fibroblasts enhance lung adenocarcinoma tumor formation.* Cancer Res.
54. Mathew, J.H., J.D. Goosey, and J.P. Bergmanson, *Quantified Histopathology of the Keratoconic Cornea.* Optom Vis Sci.
55. Povero, D., et al., *Liver fibrosis: a dynamic and potentially reversible process.* Histol Histopathol. **25**(8): p. 1075-91.
56. Schauer, I.G. and D.R. Rowley, *The functional role of reactive stroma in benign prostatic hyperplasia.* Differentiation.
57. Dong-Le Bourhis, X., et al., *Effect of stromal and epithelial cells derived from normal and tumorous breast tissue on the proliferation of human breast cancer cell lines in co-culture.* Int J Cancer, 1997. **71**(1): p. 42-8.

58. Hayward, S.W., et al., *Malignant transformation in a nontumorigenic human prostatic epithelial cell line.* Cancer Res, 2001. **61**(22): p. 8135-42.
59. Skobe, M. and N.E. Fusenig, *Tumorigenic conversion of immortal human keratinocytes through stromal cell activation.* Proc Natl Acad Sci U S A, 1998. **95**(3): p. 1050-5.
60. Ronnov-Jessen, L., et al., *The origin of the myofibroblasts in breast cancer. Recapitulation of tumor environment in culture unravels diversity and implicates converted fibroblasts and recruited smooth muscle cells.* J Clin Invest, 1995. **95**(2): p. 859-73.
61. Delcourt-Huard, A., et al., *Reconstituted human gingival epithelium: nonsubmerged in vitro model.* In Vitro Cell Dev Biol Anim, 1997. **33**(1): p. 30-6.
62. Gruenert, D.C., W.E. Finkbeiner, and J.H. Widdicombe, *Culture and transformation of human airway epithelial cells.* Am J Physiol, 1995. **268**(3 Pt 1): p. L347-60.
63. Minami, Y., H. Sugihara, and S. Oono, *Reconstruction of cornea in three-dimensional collagen gel matrix culture.* Invest Ophthalmol Vis Sci, 1993. **34**(7): p. 2316-24.
64. Prunieras, M., M. Regnier, and D. Woodley, *Methods for cultivation of keratinocytes with an air-liquid interface.* J Invest Dermatol, 1983. **81**(1 Suppl): p. 28s-33s.
65. Ehrhardt, C. and K.-j. Kim, *Drug absorption studies : in situ, in vitro and in silico models*. 2008, New York: Springer. xxii, 696 p.
66. Haws, C., et al., *CFTR in Calu-3 human airway cells: channel properties and role in cAMP-activated Cl- conductance.* Am J Physiol, 1994. **266**(5 Pt 1): p. L502-12.
67. Shen, B.Q., et al., *Calu-3: a human airway epithelial cell line that shows cAMP-dependent Cl- secretion.* Am J Physiol, 1994. **266**(5 Pt 1): p. L493-501.
68. Wan, H., et al., *Tight junction properties of the immortalized human bronchial epithelial cell lines Calu-3 and 16HBE14o.* Eur Respir J, 2000. **15**(6): p. 1058-68.
69. Abraham, G., et al., *Expression of functional beta2-adrenergic receptors in the lung epithelial cell lines 16HBE14o(-), Calu-3 and A549.* Biochim Biophys Acta, 2004. **1691**(2-3): p. 169-79.
70. Ehrhardt, C., et al., *Influence of apical fluid volume on the development of functional intercellular junctions in the human epithelial cell line 16HBE14o-: implications for the use of this cell line as an in vitro model for bronchial drug absorption studies.* Cell Tissue Res, 2002. **308**(3): p. 391-400.
71. Ehrhardt, C., et al., *16HBE14o- human bronchial epithelial cell layers express P-glycoprotein, lung resistance-related protein, and caveolin-1.* Pharm Res, 2003. **20**(4): p. 545-51.
72. Atsuta, J., et al., *Phenotyping and cytokine regulation of the BEAS-2B human bronchial epithelial cell: demonstration of inducible expression of the adhesion molecules VCAM-1 and ICAM-1.* Am J Respir Cell Mol Biol, 1997. **17**(5): p. 571-82.
73. Steerenberg, P.A., et al., *Diesel exhaust particles induced release of interleukin 6 and 8 by (primed) human bronchial epithelial cells (BEAS 2B) in vitro.* Exp Lung Res, 1998. **24**(1): p. 85-100.

74. Sun, W., R. Wu, and J.A. Last, *Effects of exposure to environmental tobacco smoke on a human tracheobronchial epithelial cell line.* Toxicology, 1995. **100**(1-3): p. 163-74.
75. Veranth, J.M., et al., *Cytokine responses of human lung cells (BEAS-2B) treated with micron-sized and nanoparticles of metal oxides compared to soil dusts.* Part Fibre Toxicol, 2007. **4**: p. 2.
76. Halldorsson, S., et al., *Differentiation potential of a basal epithelial cell line established from human bronchial explant.* In Vitro Cell Dev Biol Anim, 2007. **43**(8-9): p. 283-9.
77. Sheehan, D.C. and B.B. Hrapchak, *Theory and practice of histotechnology*. 2d ed. 1980, St. Louis: Mosby. xiii, 481 p., [1] leaf of plates.
78. Wu, R., et al., *Growth and differentiation of human nasal epithelial cells in culture. Serum-free, hormone-supplemented medium and proteoglycan synthesis.* Am Rev Respir Dis, 1985. **132**(2): p. 311-20.
79. Lechner, J.F., et al., *Clonal growth of normal adult human bronchial epithelial cells in a serum-free medium.* In Vitro, 1982. **18**(7): p. 633-42.
80. Whitcutt, M.J., K.B. Adler, and R. Wu, *A biphasic chamber system for maintaining polarity of differentiation of cultured respiratory tract epithelial cells.* In Vitro Cell Dev Biol, 1988. **24**(5): p. 420-8.
81. Choe, M.M., A.A. Tomei, and M.A. Swartz, *Physiological 3D tissue model of the airway wall and mucosa.* Nat Protoc, 2006. **1**(1): p. 357-62.
82. Gutierrez-Barrera, A.M., et al., *Establishment of three-dimensional cultures of human pancreatic duct epithelial cells.* Biochem Biophys Res Commun, 2007. **358**(3): p. 698-703.
83. Kim, S.S., et al., *Survival and function of hepatocytes on a novel three-dimensional synthetic biodegradable polymer scaffold with an intrinsic network of channels.* Ann Surg, 1998. **228**(1): p. 8-13.
84. Krause, S., et al., *A Novel 3D In Vitro Culture Model to Study Stromal-Epithelial Interactions in the Mammary Gland.* Tissue Eng Part C Methods, 2008. **14**(3): p. 261-71.
85. Stark, H.J., et al., *Authentic fibroblast matrix in dermal equivalents normalises epidermal histogenesis and dermoepidermal junction in organotypic co-culture.* Eur J Cell Biol, 2004. **83**(11-12): p. 631-45.
86. Varley, C.L. and J. Southgate, *Organotypic and 3D reconstructed cultures of the human bladder and urinary tract.* Methods Mol Biol. **695**: p. 197-211.
87. Paszek, M.J., et al., *Tensional homeostasis and the malignant phenotype.* Cancer Cell, 2005. **8**(3): p. 241-54.
88. Fulcher, M.L., et al., *Well-differentiated human airway epithelial cell cultures.* Methods Mol Med, 2005. **107**: p. 183-206.
89. Yamaya, M., et al., *Differentiated structure and function of cultures from human tracheal epithelium.* Am J Physiol, 1992. **262**(6 Pt 1): p. L713-24.
90. Amatangelo, M.D., et al., *Stroma-derived three-dimensional matrices are necessary and sufficient to promote desmoplastic differentiation of normal fibroblasts.* Am J Pathol, 2005. **167**(2): p. 475-88.
91. Coles, J.M., et al., *In situ friction measurement on murine cartilage by atomic force microscopy.* J Biomech, 2008. **41**(3): p. 541-8.

92. Bellusci, S., et al., *Involvement of Sonic hedgehog (Shh) in mouse embryonic lung growth and morphogenesis.* Development, 1997. **124**(1): p. 53-63.
93. Bellusci, S., et al., *Fibroblast growth factor 10 (FGF10) and branching morphogenesis in the embryonic mouse lung.* Development, 1997. **124**(23): p. 4867-78.
94. Jemal, A., et al., *Cancer statistics, 2009.* CA Cancer J Clin, 2009. **59**(4): p. 225-49.
95. Forbes, B., et al., *The human bronchial epithelial cell line 16HBE14o- as a model system of the airways for studying drug transport.* Int J Pharm, 2003. **257**(1-2): p. 161-7.
96. Grainger, C.I., et al., *Culture of Calu-3 cells at the air interface provides a representative model of the airway epithelial barrier.* Pharm Res, 2006. **23**(7): p. 1482-90.
97. Ramirez, R.D., et al., *Immortalization of human bronchial epithelial cells in the absence of viral oncoproteins.* Cancer Res, 2004. **64**(24): p. 9027-34.
98. Dass, C.R. and P.F. Choong, *GFP expression alters osteosarcoma cell biology.* DNA Cell Biol, 2007. **26**(8): p. 599-601.
99. Adachi, Y., et al., *Fibronectin production by cultured human lung fibroblasts in three-dimensional collagen gel culture.* In Vitro Cell Dev Biol Anim, 1998. **34**(3): p. 203-10.
100. Abraham, L.C., et al., *Guide to collagen characterization for biomaterial studies.* J Biomed Mater Res B Appl Biomater, 2008. **87**(1): p. 264-85.
101. Paquette, J.S., et al., *Production of tissue-engineered three-dimensional human bronchial models.* In Vitro Cell Dev Biol Anim, 2003. **39**(5-6): p. 213-20.
102. Vaughan, M.B., et al., *A three-dimensional model of differentiation of immortalized human bronchial epithelial cells.* Differentiation, 2006. **74**(4): p. 141-8.
103. Liu, X., et al., *Human bronchial epithelial cells can contract type I collagen gels.* Am J Physiol, 1998. **274**(1 Pt 1): p. L58-65.
104. Mio, T., et al., *Human bronchial epithelial cells modulate collagen gel contraction by fibroblasts.* Am J Physiol, 1998. **274**(1 Pt 1): p. L119-26.
105. Zhu, Y.K., et al., *Effect of initial collagen concentration on fibroblast mediated contraction of collagen gels.* Chest, 2000. **117**(5 Suppl 1): p. 234S-5S.
106. James, A.L., P.D. Pare, and J.C. Hogg, *Effects of lung volume, bronchoconstriction, and cigarette smoke on morphometric airway dimensions.* J Appl Physiol, 1988. **64**(3): p. 913-9.
107. Gunst, S.J. and J.Q. Stropp, *Pressure-volume and length-stress relationships in canine bronchi in vitro.* J Appl Physiol, 1988. **64**(6): p. 2522-31.
108. Weinberger, S.E., *Principles of pulmonary medicine*. 2nd ed. 1992, Philadelphia: Saunders. ix, 353 p.
109. Ressler, B., et al., *Molecular responses of rat tracheal epithelial cells to transmembrane pressure.* Am J Physiol Lung Cell Mol Physiol, 2000. **278**(6): p. L1264-72.
110. Khachigian, L.M., et al., *Egr-1-induced endothelial gene expression: a common theme in vascular injury.* Science, 1996. **271**(5254): p. 1427-31.

111. Khachigian, L.M., A.J. Williams, and T. Collins, *Interplay of Sp1 and Egr-1 in the proximal platelet-derived growth factor A-chain promoter in cultured vascular endothelial cells.* J Biol Chem, 1995. **270**(46): p. 27679-86.
112. Raeburn, D. and S.E. Webber, *Proinflammatory potential of the airway epithelium in bronchial asthma.* Eur Respir J, 1994. **7**(12): p. 2226-33.
113. Chau, D.Y., et al., *The cellular response to transglutaminase-cross-linked collagen.* Biomaterials, 2005. **26**(33): p. 6518-29.
114. Orban, J.M., et al., *Crosslinking of collagen gels by transglutaminase.* J Biomed Mater Res A, 2004. **68**(4): p. 756-62.
115. Siegel, R.C., S.R. Pinnell, and G.R. Martin, *Cross-linking of collagen and elastin. Properties of lysyl oxidase.* Biochemistry, 1970. **9**(23): p. 4486-92.
116. Kumaki, F., et al., *Telomerase activity and expression of human telomerase RNA component and human telomerase reverse transcriptase in lung carcinomas.* Hum Pathol, 2001. **32**(2): p. 188-95.
117. Costa, C., et al., *CXCR3 and CCR5 chemokines in induced sputum from patients with COPD.* Chest, 2008. **133**(1): p. 26-33.
118. Manicone, A.M., et al., *CXCR3 ligands contribute to Th1-induced inflammation but not to homing of Th1 cells into the lung.* Exp Lung Res, 2008. **34**(7): p. 391-407.
119. Medoff, B.D., et al., *CXCR3 and its ligands in a murine model of obliterative bronchiolitis: regulation and function.* J Immunol, 2006. **176**(11): p. 7087-95.
120. Nie, L., et al., *Attenuation of acute lung inflammation induced by cigarette smoke in CXCR3 knockout mice.* Respir Res, 2008. **9**: p. 82.
121. Emami, N. and E.P. Diamandis, *Utility of kallikrein-related peptidases (KLKs) as cancer biomarkers.* Clin Chem, 2008. **54**(10): p. 1600-7.
122. Caso, G., C. Barry, and G. Patejunas, *Dysregulation of CXCL9 and reduced tumor growth in Egr-1 deficient mice.* J Hematol Oncol, 2009. **2**: p. 7.
123. Giard, D.J., et al., *In vitro cultivation of human tumors: establishment of cell lines derived from a series of solid tumors.* J Natl Cancer Inst, 1973. **51**(5): p. 1417-23.
124. Lieber, M., et al., *A continuous tumor-cell line from a human lung carcinoma with properties of type II alveolar epithelial cells.* Int J Cancer, 1976. **17**(1): p. 62-70.
125. Nardone, L.L. and S.B. Andrews, *Cell line A549 as a model of the type II pneumocyte. Phospholipid biosynthesis from native and organometallic precursors.* Biochim Biophys Acta, 1979. **573**(2): p. 276-95.
126. Smith, B.T., *Cell line A549: a model system for the study of alveolar type II cell function.* Am Rev Respir Dis, 1977. **115**(2): p. 285-93.
127. Bruckner, A., et al., *Endogenous receptor-bound urokinase mediates tissue invasion of the human lung carcinoma cell lines A549 and Calu-1.* Cancer Res, 1992. **52**(11): p. 3043-7.
128. Filderman, A.E., et al., *Macrophage colony-stimulating factor (CSF-1) enhances invasiveness in CSF-1 receptor-positive carcinoma cell lines.* Cancer Res, 1992. **52**(13): p. 3661-6.
129. Sherr, C.J., *Regulation of mononuclear phagocyte proliferation by colony-stimulating factor-1.* Int J Cell Cloning, 1990. **8 Suppl 1**: p. 46-60; discussion 60-2.
130. Sherr, C.J., *Colony-stimulating factor-1 receptor.* Blood, 1990. **75**(1): p. 1-12.

131. Stanley, E.R., et al., *Biology and action of colony--stimulating factor-1.* Mol Reprod Dev, 1997. **46**(1): p. 4-10.
132. Stanley, E.R., et al., *The biology and action of colony stimulating factor-1.* Stem Cells, 1994. **12 Suppl 1**: p. 15-24; discussion 25.
133. Geissmann, F., et al., *Development of monocytes, macrophages, and dendritic cells.* Science. **327**(5966): p. 656-61.
134. Brody, A.R. and J.E. Craighead, *Cytoplasmic inclusions in pulmonary macrophages of cigarette smokers.* Lab Invest, 1975. **32**(2): p. 125-32.
135. O'Brien, A.D., et al., *Chemotaxis of alveolar macrophages in response to signals derived from alveolar epithelial cells.* J Lab Clin Med, 1998. **131**(5): p. 417-24.
136. Mantovani, A., et al., *Inflammation and cancer: breast cancer as a prototype.* Breast, 2007. **16 Suppl 2**: p. S27-33.
137. Whitworth, P.W., et al., *Macrophages and cancer.* Cancer Metastasis Rev, 1990. **8**(4): p. 319-51.
138. Zimmermann, H.W., et al., *Interleukin-8 is activated in patients with chronic liver diseases and associated with hepatic macrophage accumulation in human liver fibrosis.* PLoS One. **6**(6): p. e21381.
139. Jemal, A., et al., *Cancer statistics, 2008.* CA Cancer J Clin, 2008. **58**(2): p. 71-96.
140. Mountain, C.F. and K.E. Hermes, *Surgical treatment of lung cancer. Past and present.* Methods Mol Med, 2003. **75**: p. 453-87.
141. Ihde, D.C. and J.D. Minna, *Non-small cell lung cancer. Part II: Treatment.* Curr Probl Cancer, 1991. **15**(3): p. 105-54.
142. Andreescu, S., O.A. Sadik, and D.W. McGee, *Effect of natural and synthetic estrogens on a549 lung cancer cells: correlation of chemical structures with cytotoxic effects.* Chem Res Toxicol, 2005. **18**(3): p. 466-74.
143. Marquez-Garban, D.C., et al., *Estrogen receptor signaling pathways in human non-small cell lung cancer.* Steroids, 2007. **72**(2): p. 135-43.
144. Stabile, L.P., et al., *Human non-small cell lung tumors and cells derived from normal lung express both estrogen receptor alpha and beta and show biological responses to estrogen.* Cancer Res, 2002. **62**(7): p. 2141-50.
145. Soto, A.M., et al., *The E-SCREEN assay as a tool to identify estrogens: an update on estrogenic environmental pollutants.* Environ Health Perspect, 1995. **103 Suppl 7**: p. 113-22.
146. Snyder, S.L. and P.Z. Sobocinski, *An improved 2,4,6-trinitrobenzenesulfonic acid method for the determination of amines.* Anal Biochem, 1975. **64**(1): p. 284-8.
147. Holmes, T.C., et al., *Extensive neurite outgrowth and active synapse formation on self-assembling peptide scaffolds.* Proc Natl Acad Sci U S A, 2000. **97**(12): p. 6728-33.
148. Semino, C.E., et al., *Entrapment of migrating hippocampal neural cells in three-dimensional peptide nanofiber scaffold.* Tissue Eng, 2004. **10**(3-4): p. 643-55.
149. Chao, P.H., et al., *Silk hydrogel for cartilage tissue engineering.* J Biomed Mater Res B Appl Biomater. **95**(1): p. 84-90.
150. Kim, U.J., et al., *Three-dimensional aqueous-derived biomaterial scaffolds from silk fibroin.* Biomaterials, 2005. **26**(15): p. 2775-85.
151. Kim, U.J., et al., *Structure and properties of silk hydrogels.* Biomacromolecules, 2004. **5**(3): p. 786-92.

152. Mandal, B.B., et al., *Multilayered silk scaffolds for meniscus tissue engineering.* Biomaterials.
153. Nazarov, R., H.J. Jin, and D.L. Kaplan, *Porous 3-D scaffolds from regenerated silk fibroin.* Biomacromolecules, 2004. **5**(3): p. 718-26.